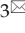

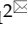



## Review

# Advances in nanomedicine for cancer starvation therapy

Shuangjiang Yu<sup>1,3</sup>, Zhaowei Chen<sup>2</sup>, Xuan Zeng<sup>2</sup>, Xuesi Chen<sup>3</sup>, Zhen Gu<sup>2</sup>

1. College of Material, Chemistry and Chemical Engineering, Hangzhou Normal University, Hangzhou 311121, P. R. China.
2. Department of Bioengineering, Jonsson Comprehensive Cancer Center, California Nanosystems Institute (CNSI), and Center for Minimally Invasive Therapeutics, University of California, Los Angeles, CA 90095, USA.
3. Key Laboratory of Polymer Ecomaterials, Changchun Institute of Applied Chemistry, Chinese Academy of Sciences, Changchun 130022, China. E-mail:

 Corresponding author: Zhen Gu, E-mail: guzhen@ucla.edu Shuangjiang Yu, E-mail: yusj@hznu.edu.cn or Xuesi Chen, E-mail: xschen@ciac.ac.cn

© The author(s). This is an open access article distributed under the terms of the Creative Commons Attribution License (<https://creativecommons.org/licenses/by/4.0/>). See <http://ivyspring.com/terms> for full terms and conditions.

Received: 2019.07.08; Accepted: 2019.09.25; Published: 2019.10.17

## Abstract

Abnormal cell metabolism with vigorous nutrition consumption is one of the major physiological characteristics of cancers. As such, the strategy of cancer starvation therapy through blocking the blood supply, depleting glucose/oxygen and other critical nutrients of tumors has been widely studied to be an attractive way for cancer treatment. However, several undesirable properties of these agents, such as low targeting efficacy, undesired systemic side effects, elevated tumor hypoxia, induced drug resistance, and increased tumor metastasis risk, limit their future applications. The recent development of starving-nanotherapeutics combined with other therapeutic methods displayed the promising potential for overcoming the above drawbacks. This review highlights the recent advances of nanotherapeutic-based cancer starvation therapy and discusses the challenges and future prospects of these anticancer strategies.

Key words: drug delivery, nanomedicine, cancer starvation therapy, combination treatment

## 1. Introduction

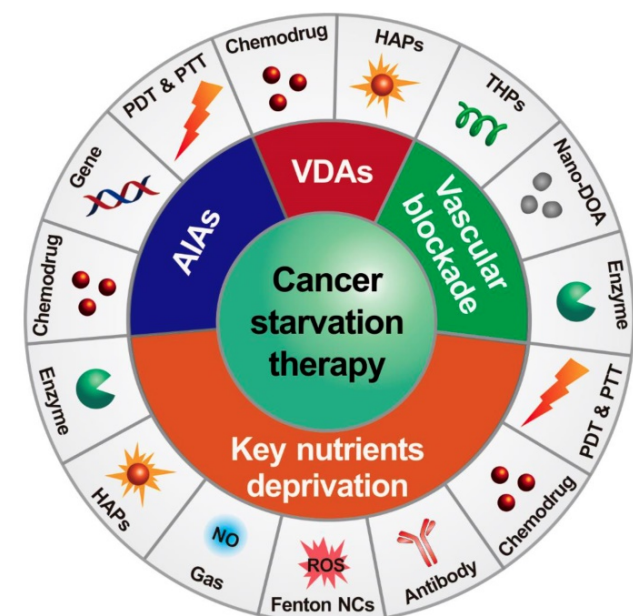
Characterized by abnormal cell metabolism and growth with risk of metastasis, cancer remains a global fatal threat to human health today [1, 2]. In recent years, cancer starvation therapy is emerging as an effective method for suppressing tumor growth and survival through blocking blood flow or depriving their essential nutrients/oxygen supply [3-5]. The transport of nutrients could be blocked by stopping the tumor blood supply with the treatments of angiogenesis inhibiting agents (AIAs) [6, 7], vascular disrupting agents (VDAs) [8, 9] and transarterial chemoembolization (TACE) [10]. Moreover, agents that could consume the intratumoral nutrients/oxygen or mediate the essential substances uptake by tumor cells can also lead to tumor "starvation" and necrosis [4, 5, 11, 12]. Although some unique advantages have been exhibited for cancer treatment these years, concerns associated with these agents, such as low targeting efficiency, elevated tumor hypoxia, acute coronary syndromes, abnormal ventricular conduction,

induced drug resistance and increased tumor metastasis risk, limit their further applications in clinic [13-16].

To overcome these challenges, combination therapy of cancer starvation agents with other cancer treating approaches has demonstrated to be an efficient way, which can maximize the therapeutic efficiency when compared to the single therapeutic method alone [17]. However, issues of the free drugs, such as undesirable drug absorption, poor bioavailability and rapid metabolism *in vivo*, have still been concerned [18]. The advances in micro-/nanotechnology as well as cancer biology have boosted development of drug delivery systems for cancer management with enhanced efficacy and limited side effects [19-22]. Among them, a variety of nanomaterials based on natural/synthetic polymers [23-29], liposomes [30], metal-organic frameworks (MOFs) [13], gold nanoparticles (NPs) [31] and silica NPs [11, 32, 33] have been employed to co-deliver cancer-starving agents and other therapeutics with

the aim of reducing drug side effects [23], improving their targeting efficacy [26, 27], increasing the stability and half-life of therapeutics [13], and co-delivery of multiple drugs to overcome the drug resistance [34, 35]. Furthermore, cancer-starvation strategy associated with the multimodal nanomedicines have also been developed for achieving synergistic cancer therapy, which has been demonstrated to be the efficient way for overcoming the side effects of free drugs and resulting in superadditive therapeutic effects [14, 15, 20].

There are two major mechanisms in designing starving-nanotherapeutics. One is stopping/reducing the tumor blood supply through inhibiting/disrupting angiogenesis, or directly blocking the blood vessels [11, 23, 26, 36, 37]. The other is depriving essential nutrients/oxygen input of tumor cells through consuming the intratumoral nutrients/oxygen, or limiting the critical nutrients uptake [4, 38-40]. For maximizing the therapeutic efficiency, these therapeutics were cooperated with other cancer treating approaches, including chemotherapy [41, 42], gene therapy [43], phototherapy [44, 45], gas therapy [46], and immunotherapy [47]. Herein, we overview the recent efforts of leveraging nanomedicine-based drug delivery systems for cancer starvation therapy and focus on the major strategies of multimodal synergistic starvation treatments (Figure 1). Both the design principles and their anticancer performance of these formulations are highlighted. Finally, the challenges and future prospects of this field are discussed.



**Figure 1.** Schematic illustration of nanomedicine-mediated cancer starvation therapy. AIA: angiogenesis inhibiting agent; Nano-DOA: nano-deoxygenation agent; HAP: hypoxia-activated prodrug; NO: nitric oxide; NC: nanocatalyst; PDT: photodynamic therapy; PTT: photothermal therapy; ROS: reactive oxygen species; THP: tumor-homing peptide; VDA: vascular disrupting agent.

## 2. Nanomedicine-mediated cancer starvation therapy

### 2.1 Antiangiogenesis-related cancer starvation therapy

Tumor growth and metastasis highly depend on the angiogenesis, which is an essential step of neoplasms from benign to malignant transformation [48]. Anti-angiogenic therapy provides an efficient way for arresting the tumor growth through inhibiting the key angiogenic activators [7, 49]. Several AIAs have been approved by the Food and Drug Administration (FDA) for clinical cancer treatment since 2003 [7]. However, associated toxicities of these AIAs are nonnegligible according to the clinical/preclinical investigation, which includes hypertension, vascular contraction, regression of blood vessels and proteinuria [14, 17, 50].

#### 2.1.1 Nano-antiangiogenesis-based cancer monotherapy

Compared to the free AIAs, nanomedicine could both improve their therapeutic outcomes *via* regulating their release behavior and increasing the drug accumulation in the tumor site through the enhanced permeability and retention (EPR) effect as well as actively targeting the tumor and/or endothelial cells *via* surface conjugation with target ligands [51, 52]. For example, mesoporous silica nanoparticles (MSNs) could significantly improve the targeting efficacy of tanshinone IIA (an angiogenesis inhibitor) to HIF-1 $\alpha$  overexpression, leading to improved antiangiogenesis activity in a mouse colon tumor model (HT-29) [53]. Several over-expressed receptors, such as integrin  $\alpha_v\beta_3$  and Neuropilin-1, were employed as the targets of nanomedicines, which showed enhanced targeting efficacy and improved tumor inhibiting rate [54-56]. Furthermore, paclitaxel (PTX) loaded antiangiogenic polyglutamic acid (PGA)-PTX-E-[c(RGDfK) $_2$ ] nano-scaled conjugate could markedly suppress the growth and proliferation of the  $\alpha_v\beta_3$ -expressing endothelial cells (ECs) and several cancer cells [57]. Additionally, bevacizumab, an angiogenesis inhibitor against vascular endothelial growth factor (VEGF) was directly used as a targeting ligand to modify magnetic iron oxide nanoparticles (IONPs), which was demonstrated to be an efficient platform for bevacizumab delivery in mice breast tumor (4T1) treatment [58].

Nanonization strategies for AIAs not only could reduce their associated toxicities and enhance the antitumor efficacy to some degree, but also provide a multidrug co-delivery platform toward enhancing the AIAs-based combination anticancer efficacy [31, 34,

59-61].

### 2.1.2 Synergistic antiangiogenesis/chemotherapy

Angiogenesis inhibitors were often used together with chemotherapeutics for overcoming their shortages and enhancing the antitumor efficacy [17]. Recently, types of engineered anti-angiogenic nanotherapeutics have been developed for cancer combination treatment. For instance, doxorubicin (DOX) and mitomycin C (MMC) co-loaded polymer-lipid hybrid nanoparticles could significantly increase the animal survival and tumor cure rate compared with liposomal DOX for treating multidrug resistant human mammary tumor xenografts [34]. DOX combining with methotrexate (MTX), which was co-delivered by MSNs could also significantly improve the efficacy of oral squamous cell carcinoma treatment through down-regulating the expression of lymph dissemination factor (VEGF-C) [62]. Zhu and coworkers synthesized a matrix metalloproteinase-2 (MMP-2)-responsive nanocarrier for the co-delivery of camptothecin (CPT) and sorafenib, which was demonstrated to be an efficient approach for colorectal cancer synergistic therapy [63]. Curcumin (Cur), a potent antiangiogenesis agent, was co-loaded with DOX into pH-responsive poly(beta-amino ester) copolymer NPs for the 4T1 tumor treatment, which showed intensive anti-angiogenic and pro-apoptotic activities [64].

### 2.1.3 Synergistic antiangiogenesis/gene therapy

The co-delivery of antiangiogenesis drugs and gene silencing agents is considered to be another efficient way for cancer starvation therapy [43, 65-67]. For example, Lima and coworkers synthesized a chlorotoxin (CTX)-conjugated liposomes for anti-miR-21 oligonucleotides delivery, which promoted the efficiency of miR-21 silencing and enhanced the antitumor activity with less systemic immunogenicity [68]. Liu *et al.* also found that the fusion suicide gene ( $\gamma$ CDglyTK) could induce tumor cell apoptosis more effectively after co-delivering with VEGF siRNA by a calcium phosphate nanoparticles (CPNPs), where the density of capillary vessels was also observed to obviously decrease in the xenograft tissue of gastric carcinoma (SGC7901) [67]. Furthermore, the poly-VEGF siRNA/thiolated-glycol chitosan nanocomplexes were employed to help overcome the resistant problem of bevacizumab by Kim and coworkers [65]. The results indicated that the combination of these two VEGF inhibitors produced synergistic effects with decreased VEGF expression and drug resistance.

### 2.1.4 Synergistic antiangiogenesis/phototherapy

Nanomaterial-based phototherapies that can

selectively kill cancer cells without normal tissue injury have attracted extensive interest in the field of cancer treatments [69-71]. Enhanced antitumor efficacy was also observed when angiogenesis inhibitors and phototherapy agents were combined [31, 72]. For example, Kim and coworkers developed a hybrid RNAi-based AuNP nanoscale assembly (RNAi-AuNP) for combined antiangiogenesis gene therapy and photothermal ablation (**Figure 2**) [31]. AuNPs modified by single sense/anti-sense RNA strands could self-assemble into various geometrical nanoconstructs (RNAi-AuNP). Then, PEI/RNAi-AuNP complexes were prepared with branched polyethylenimine (BPEI) for the purpose of effective intracellular delivery. After intratumoral administration, the therapeutic effects of PEI/RNAi-AuNP complexes could be activated by continuous-wavelength lasers or high intensity focused ultrasound, which led to effective antiangiogenesis and tumor ablation. In another work, a carrier-free nanodrug was prepared by self-assembling of Sorafenib and chlorin e6 (Ce6) for antiangiogenesis and photodynamic therapy [72]. This nanodrug presented good passive targeting behavior in the tumor sites and effective reactive oxygen species (ROS) generation ability *in vivo*. The tumor inhibition rate was significantly improved after combination with Sorafenib. With additional merits, such as good biosafety and biocompatibility, this nano-integrated strategy promised potential for cancer synergetic treatment in clinic.

## 2.2 VDAs-based cancer starvation therapy

VDAs, as a unique class of anticancer compounds, is designed to selectively prevent the established abnormal tumor blood vasculature by targeting ECs and pericytes, leading to tumor starvation and central necrosis through hypoxia and nutrient deprivation [73]. However, they are powerless to the cancer cells at the tumor margin, which could draw oxygen and nutrients from the surrounding normal tissues [15]. Beside this, several other vascular risk factors, such as the acute coronary syndromes, blood pressure alteration, abnormal ventricular conduction, and transient flush, also limit the further application of free VDAs [73]. To overcome the above issues and enhance their antitumor ability, VDAs-based multimodal cancer therapies have been developed for solid tumor treatments [23, 27, 28, 42, 74-78].

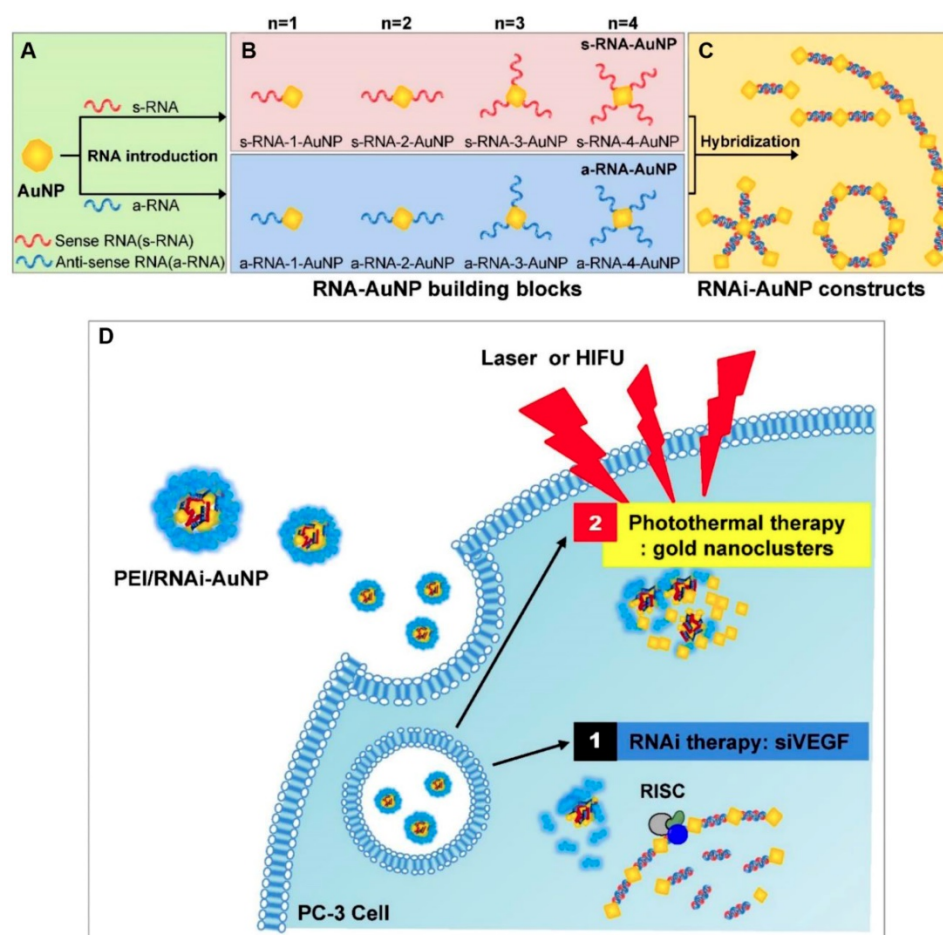
### 2.2.1 Free VDAs-enhanced nanomedicine-based chemotherapy

The barriers of heterogeneity and high interstitial fluid pressure of solid tumors not only

limit the targeting efficiency of nanomedicines, but also weaken their antitumor ability against the tumor central area [79, 80]. Recent studies reported that small free molecule VDAs could help nanomedicines to overcome the above drawbacks [42, 74, 75]. For example, Chen and coworkers developed a coadministration strategy using free CA4P and CDDP-loaded PLG-g-mPEG NPs (CDDP-NPs) for complementing each other's antitumor advantages and improving the antitumor efficiency [75]. The multispectral optoacoustic tomography (MSOT) images indicated that the tumor penetration of CDDP-NPs highly relied on the tumor vasculature, which aggregated in the peripheral region of the tumors. While co-administration of free CA4P and CDDP-NPs improved the tumor cellular killing efficiency both in the central and peripheral regions according to hematoxylin and eosin (H&E) staining. The enhanced antitumor efficiency against both murine colon cancer (C26) and human breast cancer (MDA-MB-435) models supported that this combination strategy was a promising way for solid tumor treatment.

Furthermore, small molecule VDAs could induce

tumor target amplification of ligand-coated NPs through selectively modifying tumor vasculature. For example, protein p32, a stress-related protein which is specifically expressed on the surface of tumor cells [37], can selectively bind with the phage-displayed cyclic peptide (LyP-1) [81]. Ombrabulin, a small molecule VDAs, was used to induce the local upgraded presentation of protein p32 for enhancing the tumor "active targeting" of LyP-1 coated NPs. The *in vivo* results demonstrated that the recruitment of LyP-1 coated DOX-loaded NPs significantly increased after pretreating with ombrabulin when compared with the control groups [74]. In another work, coagulation-targeted polypeptide-based NPs were developed for improving their tumor-targeting accumulation by homing to VDA-induced artificial coagulation environment. The *in vivo* results showed that this cooperative targeting system recruited over 7-fold higher CDDP doses to the tumors than non-cooperative control groups [42]. The above cooperative targeting strategies combining with free VDAs and ligand-coated NPs showed obviously decreased tumor burden and prolonged mice survival compared to the non-cooperative controls.



**Figure 2.** Schematic illustration of antisense- and sense-RNA strands introduction (A), RNA-AuNP building blocks with n-designated numbers of RNA strands (B) and versatile RNAi-AuNP nanoconstructs (C). Illustration of PEI/RNAi-AUNPs-induced the combinational strategy of anti-angiogenesis/photothermal cancer therapy (D). Reproduced with permission from ref. [31]. Copyright 2017, Ilyspring international publisher.

## 2.2.2 VDAs-nanomedicine induced synergistic starvation/chemotherapy

VDAs-nanomedicine could enhance their accumulation and retention at the leaky tumor vasculature *via* EPR effect, leading to high distribution and gradual release of VDAs around the immature tumor blood vessels as well as prolonged vascular disruption effect compared to free drugs [28]. Beside this, nanomedicine also provides a platform for VDAs-based cancer multimodal therapy [23, 27, 76, 78]. For instance, a multi-compartmental “nanocell” integrating a DOX-PLGA conjugate core and a phospholipid shell was prepared for achieving temporal release of DOX and combretastatin A4 (CA4) [23]. After accumulating at the tumor site, CA4 was released from the outer phospholipid shell of the nanocell rapidly and attacked the tumor blood vessels, and DOX was then released subsequently from the inner polymeric core for killing tumor cells directly. This mechanism-based strategy exhibited reduced side toxicity and enhanced therapeutic synergism in the progress of inhibiting murine melanoma (B16F10) and Lewis lung carcinoma growth.

Furthermore, several polymer-VDA conjugates caused amplified TME characteristics was also utilized to develop new cancer co-administration strategies [27, 78]. Hypoxia is one of the major features of solid tumors which can promote neovascularization, drug resistance, cell invasion and tumor metastasis [82, 83]. Meanwhile, the existence of hypoxia also provides the desired target for tumor selective therapy [21]. Tirapazamine (TPZ) is a typical hypoxia-activated prodrug (HAP), which own low toxicity toward normal tissues and can selectively kill the hypoxic cells after conversion into cytotoxic benzotriazinyl (BTZ) radical within hypoxic regions [84]. Nevertheless, the insufficient hypoxia level within tumors tremendously limited its further clinical application [85]. To address this, Chen and coworkers proposed a cooperative strategy based on VDA-nanomedicine and HAPs for solid tumor treatment (**Figure 3**) [27]. In this study, poly(L-glutamic acid)-CA4 conjugate nanoparticles (CA4-NPs) were employed to selectively disrupt the abnormal vasculature of the tumor, as well as elevating the hypoxia level of the tumor microenvironment (TME). The intensive hypoxic TME further boosted the antitumor efficacy of TPZ subsequently. The *in vivo* results demonstrated that this combinational strategy can not only completely suppress the small tumor growth (initial tumor volume: 180 mm<sup>3</sup>), but also obviously keep down the size of large tumors (initial tumor volume: 500 mm<sup>3</sup>)

without distal tumor metastasis. Moreover, Chen and coworkers also demonstrated that the expression of matrix metalloproteinase 9 (MMP9, a typical tumor-associated enzyme) in treated tumors (4T1) could be markedly increased by more than 5-fold after treatment with CA4-NPs. These overexpressed MMP9 could further activate the DOX release from a MMP9-sensitive doxorubicin prodrug (MMP9-DOX-NPs) and enhance the *in vivo* cooperative antitumor efficacy [78].

## 2.3 Vascular blockade-induced cancer starvation therapy

Besides the strategies of anti-angiogenic therapy and VDAs-induced tumor blood vessel disrupting, another promising strategy for cancer starvation therapy was proposed by shutting off the blood supply with nanotherapeutics that could selectively blockade tumor vascular and then inducing tumor necrosis.

### 2.3.1 Tumor-homing peptides-induced cancer starvation therapy

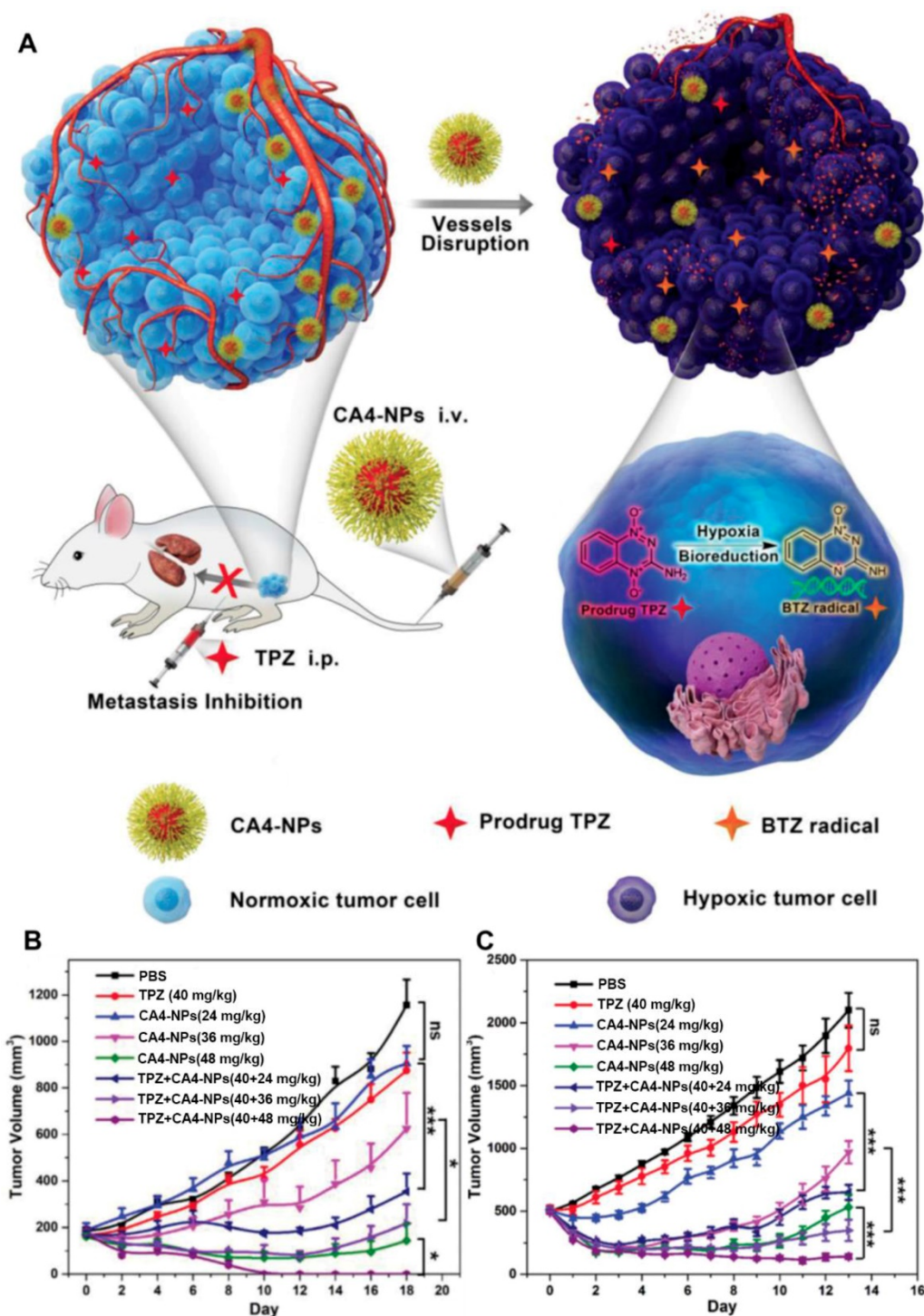
Tumor-homing peptides (THPs), such as pentapeptide (CREKA) and 9-amino acid cyclic peptide (CLT-1), could specially bind with fibrin-fibronectin complex in tumor blood clots [86]. Based on this, Ruoslahti and coworkers developed a CREKA modified IONPs for fibrin-fibronectin complexes targeting and subtle clotting in tumor vessels [87]. The initial deposition of these CREKA-IONPs created new binding sites for the subsequent NPs, and further enhanced the blood coagulation in the tumor lesion. The results indicated that the tumor imaging efficiency of this self-amplifying tumor homing system owned about six-fold enhancement compared to the control groups. However, the tumor inhibition efficiency of this system showed no significant improvement due to the insufficient tumor vessel occlusion. To this end, a cooperative theranostic system containing CREKA-IONPs and CRKDKC-coated iron oxide nanoworms was further developed by the same research group for improving the clots binding efficacy. The results proved that this combination system led to 60~70% tumor blood blockades and obvious tumor size reduction *in vivo* [88].

### 2.3.2 Thrombin-mediated cancer starvation therapy

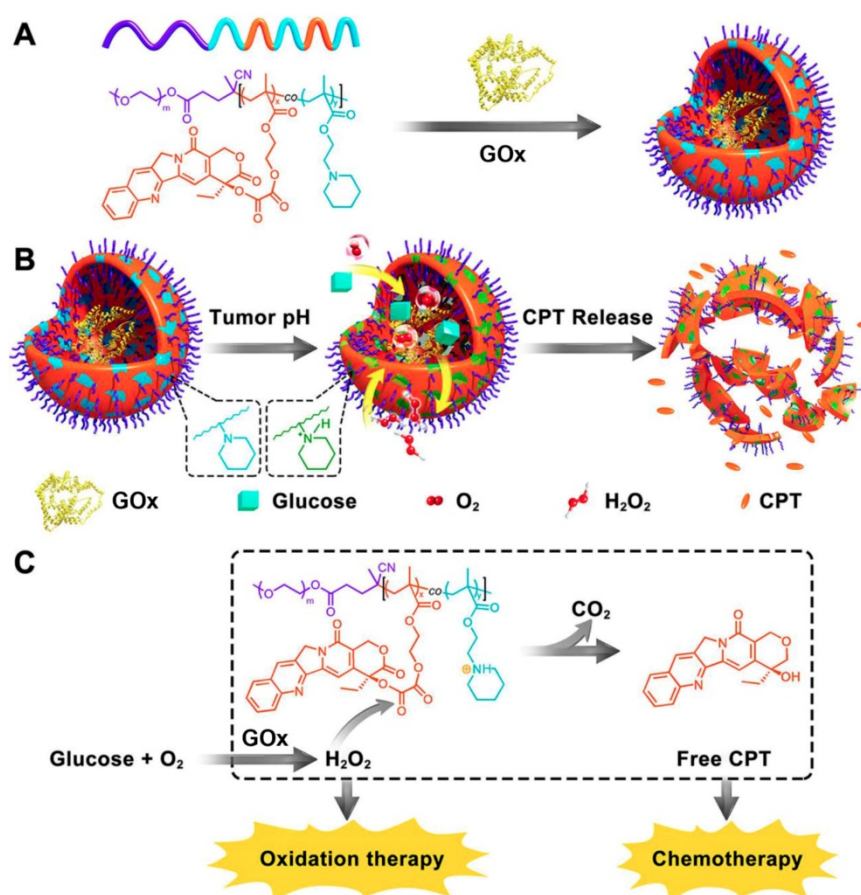
Thrombin is a serine protease that catalyzes series of coagulation-related reactions and leads to rapid thrombus formation during the clotting process [48]. If thrombin can be precisely delivered to the tumor site and lead to selective occlusion of tumor-associated vessels by inducing the local blood

coagulation, it might be a promising way for inhibiting the growth and metastasis of tumors. Recently, a nucleolin-targeting multifunctional DNA nanorobotic system was constructed for smart drug delivery. The presence of the nucleolin subsequently triggered the opening of these DNA nanotubes and released the loaded therapeutic thrombin, which then led to specific intravascular thrombosis and tumor

vessel blockade at the tumor site [26]. The growth of several tumor models was suppressed efficiently after treating with this thrombin-loaded DNA nanorobot, demonstrating that this system could become an attractive platform for cancer starvation therapy in a precise manner.



**Figure 3.** Schematic illustration of hypoxia-inducing VDA nanodrug combined with hypoxia-activated prodrug for cancer therapy (A). Tumor volume changes of BALB/c mice bearing 4T1 tumors with both moderate sizes ( $\approx 180 \text{ mm}^3$ ) ( $n=6$ ). (B). and large sizes ( $\approx 500 \text{ mm}^3$ ) ( $n=6$ ). (C). All data points are presented as mean  $\pm$  standard deviation (s.d.). (\* $P<0.05$ , \*\* $P<0.01$ , \*\*\* $P<0.001$ ). Reproduced with permission from ref. [27]. Copyright 2019, Wiley-VCH.



**Figure 4.** Schematic illustration of the preparation of GOx@PCPT-NR (A). Scheme of cancer starvation/chemotherapy via *in situ* H<sub>2</sub>O<sub>2</sub> generation and acidity-activated CPT release (B). Molecular mechanism of GOx@PCPT-NR-induced cancer starvation/chemotherapy (C). Reproduced with permission from ref. [41]. Copyright 2017, American Chemical Society.

### 2.3.3 Deoxygenation agent-induced cancer starvation therapy

It is known that insufficient oxygen (O<sub>2</sub>) supply could result in hypoxia-induced tumor cell necrosis [89]. Based on this, Zhang *et al.* designed an injectable polyvinyl pyrrolidone (PVP)-modified magnesium silicide (Mg<sub>2</sub>Si) nanoparticle as a nano-deoxygenation agent (nano-DOA) for directly consuming the intratumoral O<sub>2</sub> and starving tumors [11]. This polymer-coated Mg<sub>2</sub>Si NPs could respond to the slightly acidic TME after the intratumoral injection, and be converted into silicon dioxide (SiO<sub>2</sub>) by scavenging the surrounding O<sub>2</sub> at the tumor site. As a byproduct, the *in situ* formed SiO<sub>2</sub> aggregates further occluded the tumor capillaries and obstructed the follow-up nutrient and O<sub>2</sub> supply.

On the other hand, the intratumoral hypoxic level was also enhanced in the progress of O<sub>2</sub> consuming with the presence of DOA. Given this reason, Bu and coworkers prepared a TPZ loaded PVP-modified Mg<sub>2</sub>Si nanoparticles (TPZ-MNPs) for drug delivery and combination cancer therapy [38]. After intratumoral injection, the TPZ-MNPs quickly scavenged the O<sub>2</sub> *in situ* and created an artificial

anaerobic environment which caused the surrounding cell dormancy. Meanwhile, the released TPZ was activated in this promoted hypoxia TME, which further caused the now-dormant tumor cells death.

### 2.4 GOx-mediated cancer starvation therapy

Glucose is the major energy supplier for tumor growth and proliferation [90]. Glucose oxidase (GOx) can specifically catalyze the conversion of glucose into gluconic acid and hydrogen peroxide (H<sub>2</sub>O<sub>2</sub>) with the involvement of O<sub>2</sub>. This reaction can directly consume glucose and O<sub>2</sub>, and elevate the local acidity, hypoxia and oxidation stress *in vivo*. Given this background, GOx has aroused considerable interest for cancer diagnosis and treatment in the past decade [4, 91]. Nevertheless, there are several limitations of this approach when using GOx as an anticancer agent. On the one hand, the overproduced H<sub>2</sub>O<sub>2</sub> of glucose oxidation can cause systemic toxicity and lethal chain reactions through directly damaging cell membranes, proteins and DNA of normal cells [92, 93]. On the other hand, similar glucose supply and physiological requirement of normal cells often lead to off-targeting and ineffective starvation treatment [94]. Through nanomedicine, GOx can co-delivery with other

therapeutic agents for cancer multimodal treatments [4]. Herein, we overview the recent representative GOx-based nanomedicines for cancer starvation therapy.

#### 2.4.1 GOx-based cancer monotherapy

GOx could be used as an antitumor agent alone through consuming the intratumoral glucose and making the tumor “starving”. The continuously generated  $H_2O_2$  could further lead to DNA damage and tumor cell apoptosis [95, 96]. For example, Dinda *et al.* prepared a GOx-entrapped biotinylated vesicle for active targeting cancer starvation therapy [97]. This GOx-containing system showed about six-fold higher tumor cell killing efficiency compared to normal cells through depleting the glucose supply for tumor cells *in vitro*. However, the glucose depletion efficiency was restrained by the hypoxic TME *in vivo*, because of the insufficient  $O_2$  supply in the solid tumor. Therefore, a hyaluronic acid (HA)-coated GOx and  $MnO_2$  coloaded nanosystem (GOx- $MnO_2$ @HA) was constructed for enhancing cancer starvation therapy outcome [98]. After uptaking by the CD44-expressing tumor cells, the local glucose was converted into gluconic acid and  $H_2O_2$  with GOx catalysis. The generated  $H_2O_2$  then reacted with  $MnO_2$  to generate  $O_2$ , which further accelerated the local glucose-consumption. This nanosystem provided benefit to break the hypoxia obstacles and enhance the antitumor effect by GOx.

#### 2.4.2 Synergistic starvation/chemotherapy

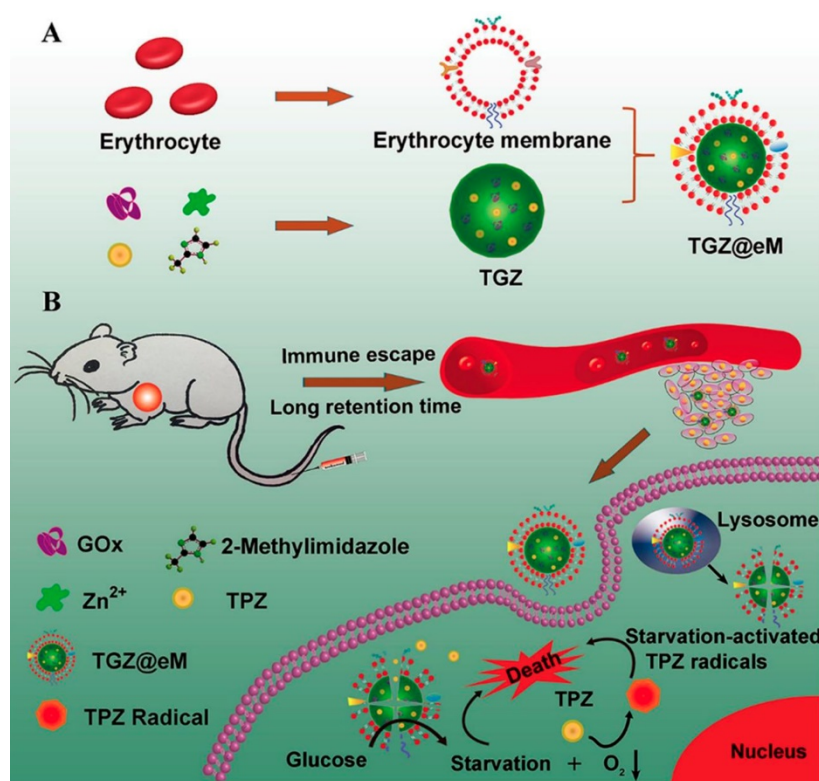
As discussed above, the concentration of generated  $H_2O_2$  can be substantially elevated in the presence of GOx at the lesion site. The increased  $H_2O_2$  level was exquisitely used to activate the  $H_2O_2$ -sensitive prodrugs for enhancing the synergistic efficiency of both cancer starvation and chemotherapy [41, 99]. For example, Li *et al.* prepared a pH-responsive prodrug-based polymersome nanoreactor (GOx@PCPT-NR) that consisted of piperidine group, camptothecin (CPT) prodrug, PEG and GOx for cancer combination therapy (Figure 4) [41]. This polymersome nanoreactor owned prolonged blood circulation and high tumor accumulation efficiency. The terminal elimination half-life of GOx@PCPT-NR reached above 39 hours after intravenous injection. This drug delivery system also showed excellent stability and almost no  $H_2O_2$  and free CPT were found within 48 h treatment in the plasma or liver. Nevertheless, the slight acidity of the tumor (pH = 6.8) could trigger the GOx release from the polymersome, which then catalyzed the conversion of intratumoral glucose into gluconic acid and  $H_2O_2$ . The enhanced acidity causing by the generated gluconic acid could further promote

the GOx release, while the elevated  $H_2O_2$  level could further accelerate the active CPT release. The accumulating effects amplified the combination antitumor efficiency [41]. Furthermore, this strategy was further confirmed by another biomimetic cascade nanoreactor (Mem@GOx@ZIF-8@BDOX) *in vivo*. As a byproduct of GOx-induced glucose depletion, gluconic acid could promote the release of loaded BDOX prodrug from the nano-framework, and the released BDOX were then converted into DOX in the presence of elevated  $H_2O_2$  at the tumor site [99].

#### 2.4.3 GOx-inducing cancer starvation and hypoxia-activated chemotherapy

The consummation of molecular oxygen could increase the local hypoxia level in the progress of GOx-involved cancer therapy. This promoted hypoxic microenvironment was also employed to activate the hypoxia-activated prodrugs and amplify their antitumor activity [13, 30, 33, 100]. For example, a MOF-based biomimetic nanoreactor coating with erythrocyte membrane (eM) was developed for precise GOx and TPZ delivery and cancer combination therapy (Figure 5) [13]. The grafted biomimetic surface of the nanoreactor not only endowed it with prolonged blood circulation and immune-escaping property, but also enhanced the tumor homing efficiency of this nanosystem. After uptake by cells, the released GOx deprived the endogenous glucose and  $O_2$ , which resulted in amplified hypoxic microenvironment and sufficient activation of TPZ. Based on the above synergistic cascade effects, a colon cancer model were efficiently inhibited *in vivo*. In another work, the PEG-modified long-circulating liposomes were used to sequentially deliver GOx and banoxantrone dihydrochloride (AQ4N, a hypoxia-activated prodrug) to tumors for cancer combination starvation/chemotherapy [30]. The *in vivo* photoacoustic image indicated that GOx-loaded liposome could obviously deplete the glucose of the tumor site, and lead to tumorous hypoxia enhancement. Under the elevated hypoxic microenvironment, the antitumor activity of the subsequent arrival liposome-AQ4N was activated by reducing low toxic AQ4N into high toxic 1,4-Bis[[2-(dimethylamino)ethyl]amino]-5,8-dihydroxyanthracene-9,10-dione (AQ4) by the series of intracellular reductases. Synergistically enhanced antitumor effect was observed on 4T1 murine breast cancer model after treating with this liposome-based GOx/AQ4N co-delivery system. These results demonstrated that combination of GOx-based cancer starvation therapy and HAP-involved hypoxia-activated chemotherapy is an effective way for solid tumor treatment.





**Figure 5.** Schematic illustration of preparation of GOx and TPZ coloaded biomimetic nanoreactor with erythrocyte membrane coating (TGZ@eM) (A). TGZ@eM nanoreactor induced cancer starvation/hypoxia-activated chemotherapy (B). Reproduced with permission from ref. [13]. Copyright 2018, American Chemical Society.

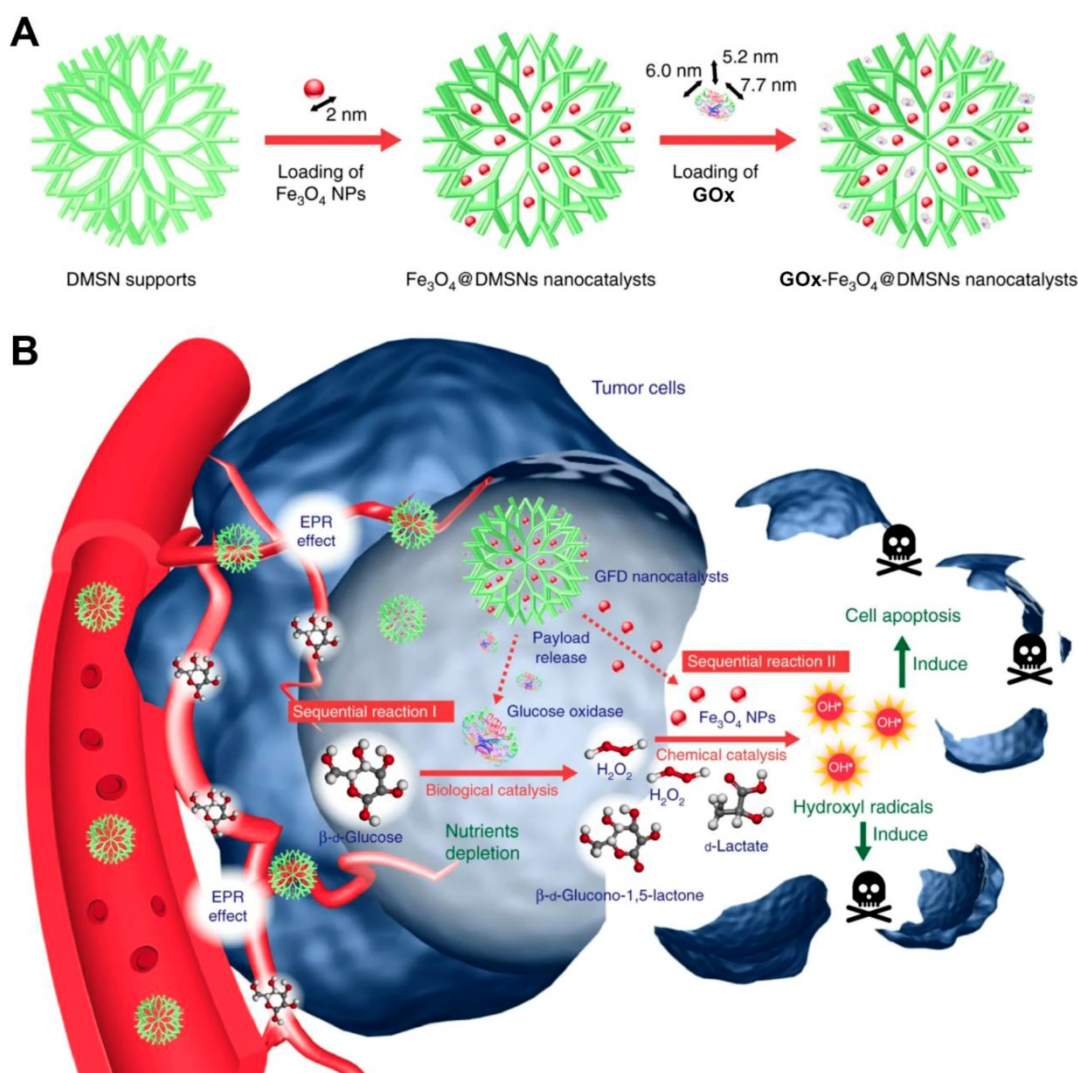
Furthermore, in order to reduce the systemic toxicity, Wang and coworkers developed a nanoclustered cascaded enzymes by crosslinking GOx and CAT with a pH-responsive block polymer poly(ethylene glycol)-*block*-poly(2-hydroxyethyl methacrylate) bearing 2-(2-carboxyethyl)-3-methylmaleic anhydride (PEG-*b*-PHEMA<sub>CMA</sub>) with a BSA/BSA<sub>TPZ</sub> (wt:wt, 1:2) outer shell for cancer starvation and hypoxia-activated chemotherapy [94]. The experimental data indicated that GOx and CAT could be released by the stimuli of the mild acidic TME after accumulating at the tumor site. Then, the release rate was self-accelerated by the subsequent generated gluconic acid with GOx-induced glucose consumption. Meanwhile, the aggravated hypoxia of TME further activated the BSA<sub>TPZ</sub> which led to hypoxia-activated chemotherapy. Importantly, the authors also found that the present CAT could timely eliminate the appeared H<sub>2</sub>O<sub>2</sub> as well as lowered the systemic toxicity of GOx-mediated cancer starvation therapy.

#### 2.4.4 Starvation/oxidation synergistic therapy

Glutathione (GSH) is a natural antioxidant in the body, which prevents the damage of important cellular components by ROS, such as H<sub>2</sub>O<sub>2</sub>, hydroxyl radicals ( $\cdot$ OH), and singlet oxygen (<sup>1</sup>O<sub>2</sub>). However, GSH could weaken the antitumor efficiency in the progress of ROS-mediated cancer therapy. To this

end, Li *et al.* prepared GOx-loaded therapeutic vesicles based on a diblock copolymer containing a mPEG segment and copolymerized piperidine-functionalized methacrylate and phenylboronic ester (mPEG-*b*-P(PBEM-*co*-PEM)) [101]. After precise activation at the tumor site, the GOx-induced enzymatic reaction caused local consumption of glucose and O<sub>2</sub> and generation of gluconic acid and H<sub>2</sub>O<sub>2</sub>. The generated H<sub>2</sub>O<sub>2</sub> not only elevated the intracellular oxidative stress, but also led to the production of quinone methide (QM), which further suppressed the antioxidant ability of the tumor cells through depleting the intracellular GSH. These cumulative anticancer effects of the therapeutic vesicles resulted in effective cancer cell death and tumor ablation.

H<sub>2</sub>O<sub>2</sub> can be transformed into the highly toxic ROS under certain conditions *in vivo* [71, 102]. For example, H<sub>2</sub>O<sub>2</sub> could be disproportionated into  $\cdot$ OH with the presence of Fenton reaction catalysts under acidic condition [103, 104]. While, in the presence of neutrophil-expressed phagocytic enzyme myeloperoxidase (MPO), H<sub>2</sub>O<sub>2</sub> and chlorine ion (Cl<sup>-</sup>) could be converted into hypochlorous acid (HClO) through the enzymatic reaction [105]. Based on this, specific strategies were developed to combine with GOx for cancer starvation/oxidation synergistic therapy [106-110].



**Figure 6.** Synthetic procedure for preparation of GOx-Fe<sub>3</sub>O<sub>4</sub>@DMSNs (A). Scheme of GOx-Fe<sub>3</sub>O<sub>4</sub>@DMSNs induced sequential catalytic-therapeutic mechanism for cancer therapy (B). Reproduced with permission from ref. [106]. Copyright 2017, Nature Publishing Group.

In a recent study, Huo *et al.* designed a dendritic silica nanoparticle-based sequential nanocatalyst for co-delivering of GOx and Fe<sub>3</sub>O<sub>4</sub> NPs (GOx-Fe<sub>3</sub>O<sub>4</sub>@DMSNs) for enhancing of combination anticancer efficiency (**Figure 6**) [106]. After EPR effect-induced accumulation of these nanocatalysts in the tumor site, the released GOx catalyzed the oxidation of the intratumoral glucose to gluconic acid and H<sub>2</sub>O<sub>2</sub> and led to tumor starvation and central necrosis. Thereafter, the generated H<sub>2</sub>O<sub>2</sub> sequentially were translated into highly toxic ·OH by Fe<sub>3</sub>O<sub>4</sub> NPs under the slightly acidic TME, which resulted in elevated oxidative stress and massive apoptosis of tumor cells. The final tumor inhibition rate of this nanomedicine by intravenous and intratumoral treatments with the same treating dose was reached to 64.7% and 68.9%, respectively. Besides this, another core-shell TME-responsive nanocatalyst, incorporated with a magnetic nanoparticle core of iron carbide (Fe<sub>5</sub>C<sub>2</sub>)-GOx and MnO<sub>2</sub>-nanoshell, was constructed by

Lin and co-workers [107]. After endocytosis by tumor cells, the MnO<sub>2</sub>-nanoshell of this nanosystem was degraded into Mn<sup>2+</sup> and O<sub>2</sub> and resulted in GOx release under the stimuli of the acidic microenvironment. The generated O<sub>2</sub> could enhance consumption of the local glucose with the presence of GOx, leading to sufficient tumor starving. Sequentially, the produced H<sub>2</sub>O<sub>2</sub> further evolved into ·OH catalyzed by Fe<sub>5</sub>C<sub>2</sub>, resulting in efficient tumor cell death. Recently, a smart autocatalytic Fenton nanosystem, consisted of GOx-loaded zeolitic imidazolate framework (ZIF) and adenosine triphosphate (ATP)-responsive metal polyphenol network (MPN) shell, was designed by Zhang *et al.* for the combination cancer therapy [108]. In tumor cells, the MPN shell was degraded into Fe<sup>3+</sup> and tannic acid (TA) and further triggered the inner GOx release under the stimuli of the overexpressed ATP. Then, the exposed GOx led to endogenous glucose consumption and H<sub>2</sub>O<sub>2</sub> accumulation. With the

presence of TA, the transition efficiency of  $\text{Fe}^{3+}$  to  $\text{Fe}^{2+}$  was accelerated, which further promoted the transformation of the generated  $\text{H}_2\text{O}_2$  into high toxic  $\cdot\text{OH}$  by Fenton reaction. These accumulating antitumor effects significantly suppressed the tumor growth.

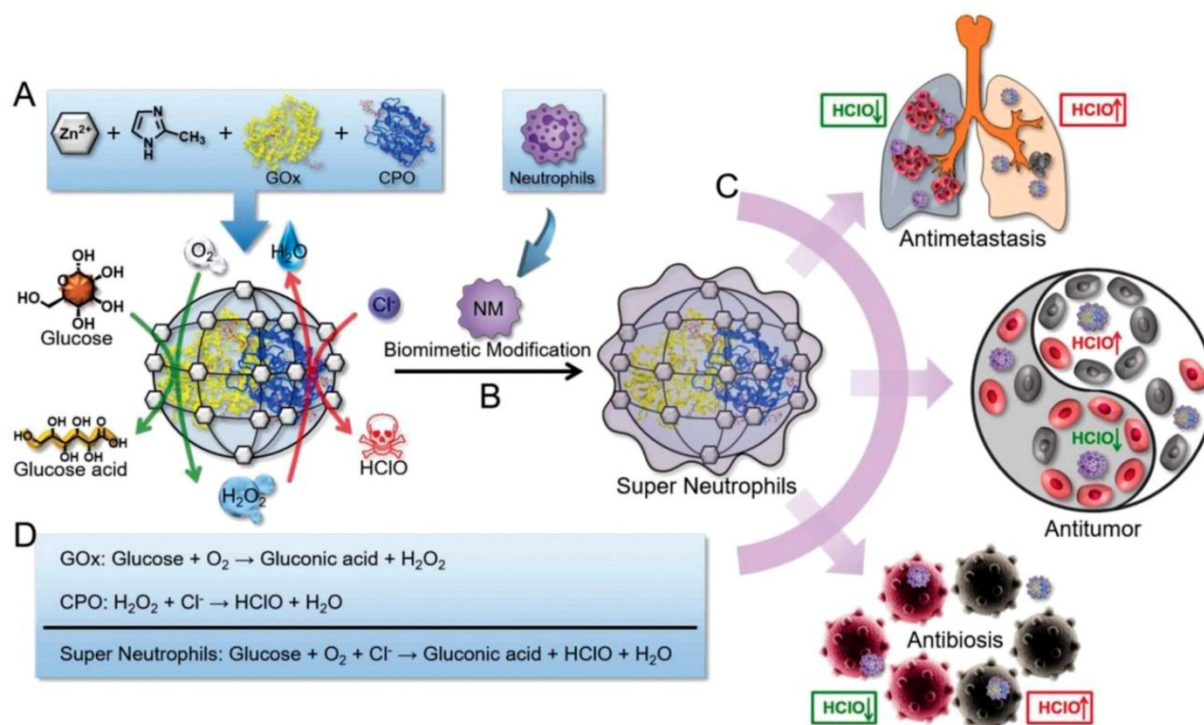
Silver (Ag) ions have been demonstrated to kill different types of cancer cells through increasing the intracellular oxidative stress, causing mitochondrial damage, and inducing cell autophagy [111, 112]. Based on this, Huang and coworkers designed a GOx-conjugated silver nanocube (AgNC-GOx) for efficient Ag ions delivery and synergistic starvation/metal-ion therapy [113]. AgNC-GOx catalyzed the glucose conversion into gluconic acid and  $\text{H}_2\text{O}_2$  after uptake by the tumor cells. Cumulative gluconic acid elevated the acidity of TME which accelerated the AgNC degradation and Ag ions generation in the tumor site. Meanwhile, the generated  $\text{H}_2\text{O}_2$  and Ag ions were found to lead the eradication of 4T1 cancer cells. Both the glucose consumption and accumulation of toxic  $\text{H}_2\text{O}_2$  and Ag ions significantly suppressed the tumor growth and prolonged the mice survival.

HClO is a powerful ROS which can be generated by the MPO-mediated catalysis and owns higher cellular toxicity in comparison with  $\text{H}_2\text{O}_2$ . It has been proved to be a promising candidate for cancer therapy through disrupting some cellular functions and

promoting the tumor cell death by the oxidation progress [114]. Given this pattern, Zhang and coworkers prepared an “artificial neutrophils”, consisting of GOx and chloroperoxidase (CPO) coloaded zeolitic imidazolate framework-8 (ZIF-8) core and neutrophil membrane (NM) coating (GOx-CPO@ZIF-8@NM), for both of cancer and infection treatments. NM coating help the NPs to target the tumor site efficiently (**Figure 7**) [109]. After uptake by the tumor cells, the embedded GOx and CPO were released from the ZIF-8 NPs, which synergistically enhanced the glucose depletion and HClO generation through a sequential enzymatic catalysis progress. According to the results, this artificial neutrophil can produced seven-fold higher reactive HClO than the natural neutrophils both *in vitro* and *in vivo*. Benefit from this, 4T1 tumors of mice was almost completely eradicated after treating with this neutrophil-mimicking NPs.

#### 2.4.5 Synergistic starvation/phototherapy

Blue light irradiation (450~490 nm) could promote the Conversion of  $\text{H}_2\text{O}_2$  into more toxic  $\cdot\text{OH}$ , which provides an alternative approach for cancer therapy. However, insufficient  $\text{H}_2\text{O}_2$  supplies in the tumor site weaken the  $\cdot\text{OH}$  production as well as the antitumor efficiency. Instead, GOx, as an antitumor agent, could induce the glucose depletion and tumor starvation with consecutively generating of  $\text{H}_2\text{O}_2$ .



**Figure 7.** Schematic representation of the synthesis of GOx and CPO-coaloead ZIF-8 NPs. Glucose conversion and HClO generation with the catalyzing of GOx and CPO (A). Preparation of the “artificial neutrophils” by the surface modification of the GOx/CPO-coaloead ZIF-8 NPs with natural neutrophil membrane (B). Compare to natural neutrophils, the “artificial neutrophils” showed stronger HClO generation ability for biomedical applications (C). The mechanism of enzymatic reaction of GOx, CPO and “artificial neutrophils” (D). Reproduced with permission from ref. [109]. Copyright 2019, Wiley-VCH.

Given this fact, Chang *et al.* developed GOx-conjugated polymer dots (Pdot-GOx) for enzyme-enhanced phototherapy (EEPT) [115]. After immobilizing into tumor, Pdot-GOx NPs could efficiently catalyze the glucose oxidation and steadily produce  $H_2O_2$ , which led to the enhancement of the local oxidative stress. Meanwhile, the appeared  $H_2O_2$  could also be photolyzed to produce  $\cdot OH$  under light irradiation (460 nm) for killing tumor cells. The experimental results indicated that this EEPT strategy exhibited much higher efficacy in inhibiting MCF-7 tumor growth compared with the control groups in mouse models.

Photodynamic therapy (PDT) has proved to be a promising platform in imaging and treatment of cancers and other diseases [116]. As a noninvasive method, PDT utilizes the generated toxic ROS to destroy the cellular organelles and ablate tumors with the presence of photosensitizers under light irradiation. However, the poor penetration of the excitation light makes it powerless against deeply seated tumors [117]. Besides, hypoxia of TME is another suppressive factor for this  $O_2$ -dependent antitumor approach [118]. Thus, the combination with other strategies would be an alternative way for improving the efficiency of PDT-involved cancer therapy [119, 120]. Recently, Li *et al.* developed a GOx and catalase co-loaded porphyrin metal-organic framework with tumor cell membrane surface coating (mCGP) for synergistic starvation/PDT therapy. This mCGP NPs owned excellent tumor homing ability due to the tumor cell membrane surface coating. After internalized by tumor cells, the loaded catalase in mCGP was found to catalyze the generated  $H_2O_2$  to disproportionate into molecular  $O_2$  and  $H_2O$ , accelerating the consumption of endogenous glucose and promoting the production of  $^1O_2$  under light irradiation. These accumulating effects obviously enhanced the *in vivo* synergistic antitumor efficiency of mCGP NPs. In another work, Yu *et al.* developed a biomimetic nanoreactor (bioNR)-based starvation/PDT strategy for effective combating deeply seated metastatic tumors [32]. The bioNR was constructed based on a GOx and Ce6 conjugated hollow mesoporous silica NPs (HMSNs) with B16F10 cell membrane coating, which was filled with bis[2,4,5-trichloro-6-(pentyloxycarbonyl)phenyl]oxalate (CPPO) and perfluorohexane (PFC) in the cavity. After homing to the tumor, the peripheral glucose was converted into gluconic acid with  $H_2O_2$ . At the same time, the appeared  $H_2O_2$  not only promoted the local oxidative stress of the tumor, but also could react with CPPO to generate chemical energy, which led to chemiluminescence resonance energy transfer-based PDT with the presence of Ce6. Furthermore, the

molecular oxygen releases from PFC further increase the antitumor efficiency of  $O_2$ -dependent GOx-involved cancer starvation therapy and PDT. It was demonstrated that the Ce6-induced PDT effect for tumor metastasis was substantially enhanced after combination with GOx-involved cancer starvation therapy.

As described above, insufficient oxygen supply in solid tumors could limit the antitumor efficiency of GOx-related therapeutics. To address this challenge, Cai and coauthors prepared a HA-conjugated porous hollow Prussian Blue NPs (PHPBNs) for facilitating GOx delivery and tumor synergistic starvation/photothermal therapy [121]. The HA shell could enhance the targeting efficiency towards CD44 overexpressing tumors. After cellular endocytosis, the released GOx catalyzed the glucose depletion by consuming  $O_2$ , and PHPBNs sequentially catalyzed the generated  $H_2O_2$  splitting into  $O_2$  and  $H_2O$  to amplify the tumor starvation effect. Furthermore, GOx-induced glucose depletion not only inhibited the tumor growth, but also suppressed the expression of heat shock proteins (HSPs), where the latter facilitated PHPBNs-mediated low-temperature photothermal treatment to reduce their resistance. The results indicated that this combinational therapeutic system could significantly repress tumor growth in mice. In another work, Tang *et al.* developed a novel BSA-directed two-dimensional (2D)  $MnO_2$  nanosheet (M-NS) by one-step method [122]. This M-NS not only owned an excellent GOx-like activity for catalyzing the local glucose oxidation, but also exhibited high photothermal conversion efficiency due to the large surface area. Furthermore, this M-NS artificial enzyme showed higher thermal stability than natural GOx. The experimental results indicated that the M-NS-induced intratumoral glucose depletion inhibited the ATP production as well as cellular HSPs expression, which promoted the sensitivity of tumors to the M-NS-mediated photothermal treatments.

#### 2.4.6 Starvation/gas synergistic therapy

Previous studies have demonstrated that nitric oxide (NO) could be used as a therapeutic gas for cancer therapy through the nitrosation of mitochondria and DNA or enhance the efficiency of PDT or radiation therapy [123, 124]. L-Arginine (L-Arg) is a natural NO donor which can release NO in the presence of inducible NO synthase enzyme (iNOS) or in the presence of  $H_2O_2$  [125, 126]. Given this reality, Fan *et al.* employed a hollow mesoporous organosilica nanoparticle (HMON) for GOx and L-Arginine co-delivery (L-Arg-HMON-GOx) and cancer starvation/gas therapy (Figure 8) [46]. After accumulating at the tumor site, the intratumoral

glucose was transformed into gluconic acid and  $H_2O_2$  by GOx. The generated  $H_2O_2$  not only killed the tumor cells directly, but also enhanced the gas therapy effect through oxidizing L-Arginine into NO in the acidic TME. The *in vivo* experimental results indicated that L-Arg-HMON-GOx treated U87MG tumor bearing mice have the best tumor ablation outcome and much longer survival rate than the control groups, indicating the significantly promoted synergistic starvation/gas therapy effects.

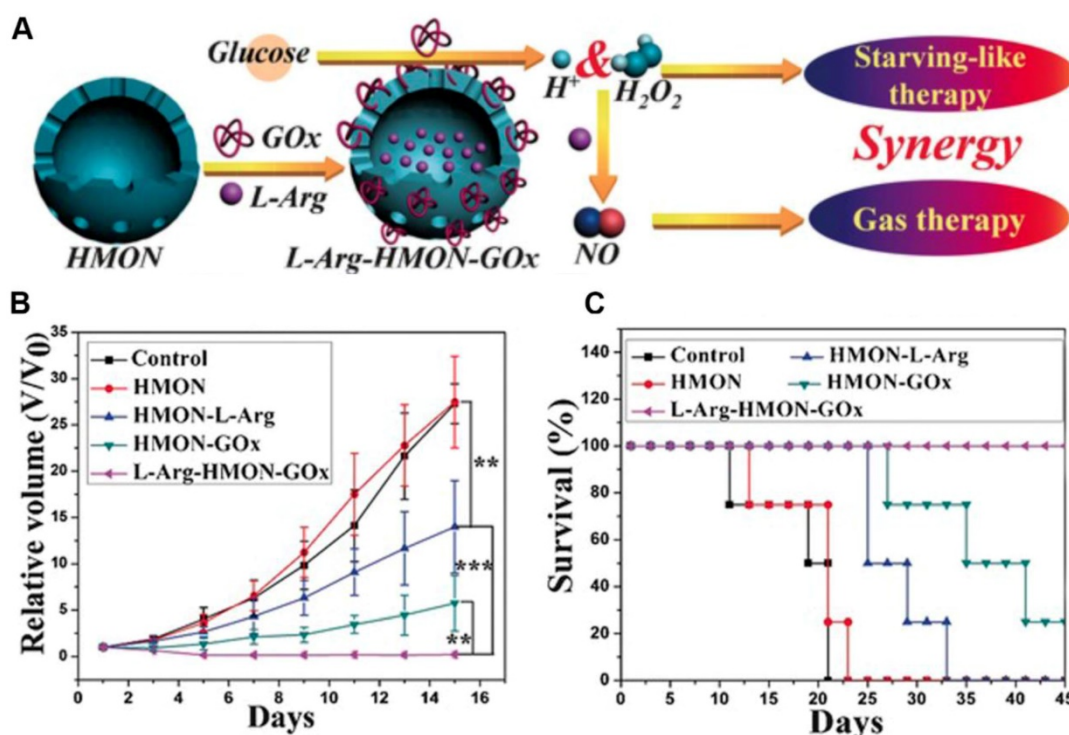
#### 2.4.7 GOx-mediated starvation/immunotherapy

Although cancer immune checkpoint blockade (ICB) therapy has been witnessed exciting progress in treating many types of cancers in clinic, several remaining challenges still need to be overcome in ICB-related cancer immunotherapy, such as low immune response efficacy, off-target side effects, and immune suppressive factors in TME [127-131]. Combination of cancer immunotherapy with other anticancer methods has been considered as an efficient strategy for addressing these issues [132-138]. For example, Xie *et al.* presented a therapeutic method combining with cancer cell membrane coated GOx-loaded mesoporous silica nanoparticles (CMSN-GOx) and anti-programmed cell death protein 1 (anti-PD-1) for cancer starvation/immunotherapy (Figure 9) [47]. Contributing to the CM coating, CMSN-GOx was efficiently delivered to the tumor site. The released GOx could not only catalyze the glucose depletion to

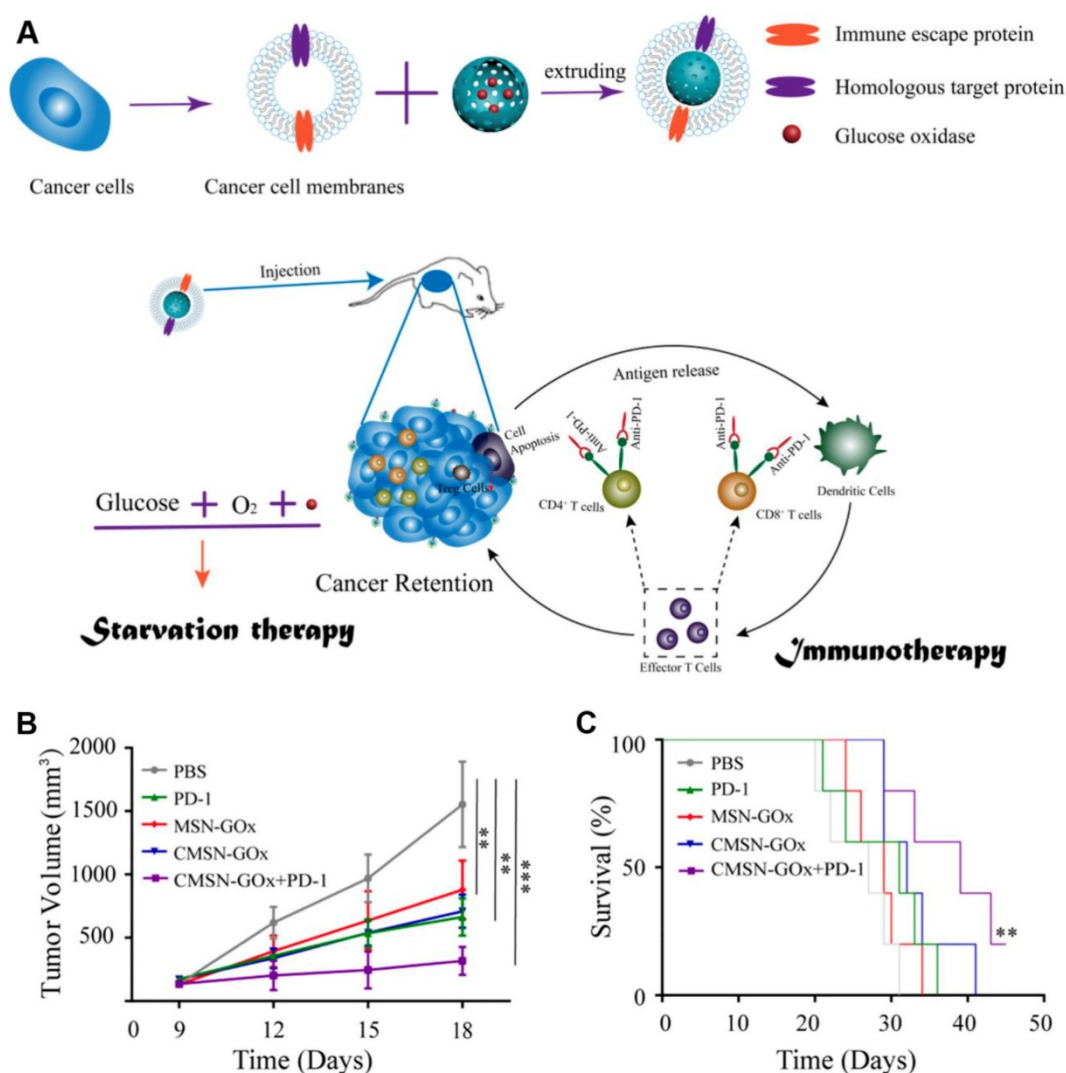
inhibit the tumor growth, but also induce more dendritic cells (DCs) maturation which further enhanced the antitumor efficacy of anti-PD-1. *In vivo* experimental results indicated that CMSN-GOx plus anti-PD-1 combination treatment provided more effective tumor suppression than any single therapies.

#### 2.4.8 GOx-involved multimodal synergistic therapy

As previously reported,  $H_2O_2$  generated in the GOx-induced glucose oxidation could split into high toxic  $\cdot OH$  radicals through Fenton reaction in the presence of  $Fe_3O_4$  [106]. The rising tumor temperature could further elevate the conversion efficiency of local  $H_2O_2$  to  $\cdot OH$  as well as enhance the antitumor ablation [71]. Given this fact, Feng *et al.* developed a  $Fe_3O_4$ /GOx co-loaded polypyrrole (PPy)-based composite nanocatalyst ( $Fe_3O_4@PPy@GOx$  NC) for multimodal cancer therapy.  $Fe_3O_4@PPy@GOx$  NCs could selectively accumulate at the tumor site (4T1) *via* EPR effect. Thereafter, the released GOx-mediated intratumoral glucose oxidation elevated the  $H_2O_2$  level and acidity of TME, which sequentially resulted in local  $\cdot OH$  accumulation and tumor cell death. At the same time, the polypyrrole (PPy) component which owned a high photothermal-conversion efficiency (66.4% in NIR-II biowindow) considerably increased the tumor temperature in both in NIR-I and NIR-II biowindows, which accelerated the  $H_2O_2$  disproportionation as well as enhanced the photothermal-enhanced cancer starvation/oxidation therapy.



**Figure 8.** The schematic illustration of the preparation of L-Arg-HMON-GOx for cancer starvation/gas synergistic therapy (A). Tumor volume changes (B) and survival curves (C) of U87 tumor bearing mice after different treatments (\* $P < 0.05$ , \*\* $P < 0.01$ , \*\*\* $P < 0.001$ ). Reproduced with permission from ref. [46]. Copyright 2017, Wiley-VCH.



**Figure 9.** Schematic illustration of CMSN-GOx induced cancer starvation/immunotherapy (A). Tumor volume changes (n=5). (B). and survival curves (n=5). (C). Of B16F10 tumor bearing mice after different treatments. All data points are presented as mean  $\pm$  standard deviation (s.d.). (\* $P < 0.05$ , \*\* $P < 0.01$ , \*\*\* $P < 0.001$ ). Reproduced with permission from ref. [47]. Copyright 2019, American Chemical Society.

## 2.5 Other strategies for cancer starvation therapy

Recently, types of special strategies in this field, which aimed at some critical nutrients, such as lactate and cholesterol, were also developed [39, 40, 139-141].

Lactate, which was once considered to be the waste product of glycolysis, has been demonstrated that can “fuel” the oxidative tumor cells growth as an energy substrate [12, 142]. Investigation indicated that interfering the lactate-fueled respiration could selectively kill the hypoxic tumor cells *via* inhibiting the expression of lactate-proton symporter, monocarboxylate transporter 1 (MCT1) [143]. Meanwhile, the reduction of lactate uptake by inhibiting the expression of MCT1 could transform the lactate-fueled aerobic respiration to anaerobic glycolysis as well as lower the O<sub>2</sub> consumption in tumor cells which would facilitate the O<sub>2</sub>-depleting

cancer therapy. For example, Zhang and coworkers developed an *a*-cyano-4-hydroxycinnamate (CHC) loaded porous Zr (IV)-based porphyrinic metal-organic framework (PZM) NPs with HA coating for cancer combination therapy (Figure 10) [40]. After effectively accumulating at the CT26 tumors, the released CHC could obviously decrease the expression of MCT1 and turn down the lactate uptake which leading to lower the O<sub>2</sub> consumption. As a result, the PDT efficiency was markedly enhanced due to the sufficient <sup>3</sup>O<sub>2</sub> converting upon the laser irradiation (600 nm). Additionally, reducing the production of lactate *via* knockdown of lactate dehydrogenase A (LDHA) in tumor cells was also demonstrated that could neutralize the tumor acidity and enhance the anti-PD-L1-mediated immunotherapy [139].

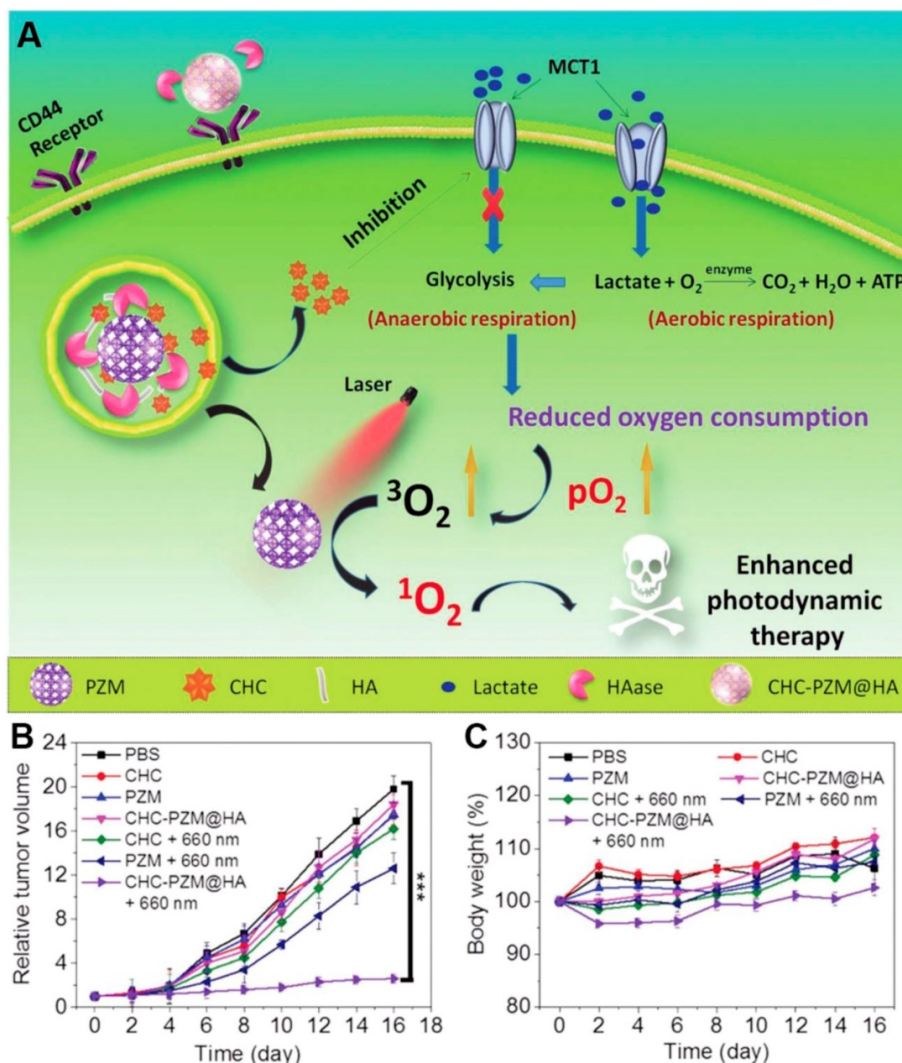
Recently, Thaxton and coworkers designed synthetic high density lipoprotein nanoparticles

(HDL-NPs) with gold NPs as a size- and shape-restrictive template for lymphoma starvation therapy [39]. This HDL-NPs could specially target scavenger receptor type B-1 (SR-B1), which is a high-affinity HDL receptor expressed by lymphoma cells. This combination of SR-B1 promoted the cellular cholesterol efflux and limited the cholesterol delivery, which selectively induced cholesterol starvation and cell apoptosis. The B-cell lymphoma growth was obviously inhibited after HDL-NPs treatment of B-cell lymphoma bearing mice. Furthermore, this HDL-NPs could reduce the activity of myeloid-derived suppressor cells (MDSCs), a type of innate immune cells that potently inhibit T cells, through specifically binding with SR-B1 of MDSCs [140]. In Lewis lung carcinoma mice model, the *in vivo* data showed that the suppression of MDSCs by HDL-NPs markedly increased CD8<sup>+</sup> T cells and reduced Treg cells in the metastatic TME. After treating with HDL-NPs, the tumor growth and metastatic tumor burden were

obviously reduced and the survival rate was clearly improved due to enhanced adaptive immunity.

### 3. Conclusion and outlook

As an attractive strategy for cancer treatment, nanomedicine-mediated cancer starvation therapy could selectively deprive the nutrients and oxygen supply through antiangiogenesis treatment, tumor vascular disrupting or blockade, direct depletion of the intratumoral glucose and oxygen, and other processes. Moreover, by combining with chemotherapeutic drugs, therapeutic genes, enzymes, metal NPs, hypoxia-activated prodrugs, inorganic NPs, Fenton-reaction catalysts, photosensitizers, or photothermal agents, two or more therapeutic agents could be readily integrated into one single formulation, leading to enhanced treatment outcomes (Table 1).



**Figure 10.** Schematic illustration of porphyrinic MOF nanoplateform mediated suppressing lactate-fueled respiration for enhanced PDT therapy (A). Tumor volume changes (n=5). (B), and body weight curves (n=5). (C). Of CT26 tumor bearing mice after different treatments. All data points are presented as mean ± standard deviation (s.d.). (\*\*\*)P < 0.001. Reproduced with permission from ref. [40]. Copyright 2018, Wiley-VCH.

**Table 1.** Representative formulations for nanomedicine-mediated cancer starvation therapy described in this review.

Strategies	Materials	Therapeutics	Administration route	Treatments	Tumor models	Ref.	
Antiangiogenesis-related cancer starvation therapy	$\alpha_v\beta_3$ -integrin targeted perfluorocarbon NPs	Docetaxel-prodrug	<i>i.v.</i> injection	Antiangiogenesis therapy	Vx2 tumor bearing rabbits	[54]	
	Chitosan NPs	Ursolic acid	Oral administration	Antiangiogenesis therapy	H22 tumor bearing mice	[145]	
	PGA-PTX-E-[c(RGDfK)] <sub>2</sub>	PTX	<i>i.v.</i> injection	Antiangiogenesis therapy	4T1 tumor bearing mice	[57]	
	Recombinant human endostatin conjugated AuNPs	Recombinant human endostatin	Subcutaneous injection	Antiangiogenesis therapy	SW620 tumor bearing mice	[146]	
	MSNs	Tanshinone IIA	<i>i.v.</i> injection	Antiangiogenesis therapy	HT-29 tumor bearing mice	[53]	
	M-MSN@PEI-PEG-KALA NPs	anti-VEGF siRNA	<i>i.v.</i> injection	Antiangiogenic gene therapy	A549 tumor bearing mice	[43]	
	$\alpha_v\beta_3$ -integrin-targeted lipid-encapsulated NPs	Fumagillin prodrug and zoledronic acid	<i>i.v.</i> injection	Dual antiangiogenic therapy	Vx2 tumor bearing rabbits	[55]	
	Thiolated-glycol chitosan formed NPs	Bevacizumab and poly- anti-VEGF siRNA	<i>i.v.</i> injection	Dual antiangiogenic therapy	A431 tumor bearing mice	[65]	
	Polymer-lipid hybrid NPs	DOX and MMC	<i>i.v.</i> injection	Antiangiogenesis therapy and chemotherapy	MDA-MB 435/LCC6/WT tumor bearing mice and MDA-MB 435/LCC6/MDR1 tumor bearing mice	[34]	
	pH and thermo-responsive MSNs	DOX and MTX	<i>i.v.</i> or oral administration	Antiangiogenesis therapy and chemotherapy	OSCC tumor bearing mice	[62]	
	PEGylated lipid bilayer-supported MSNs	AXT and CST	<i>i.v.</i> injection	Antiangiogenesis therapy and chemotherapy	SCC7 tumor bearing mice	[147]	
	MMP-2 responsive mPEG-peptide diblock copolymer (PPDC) NPs	CPT and Sorafenib	<i>i.v.</i> injection every	Antiangiogenesis therapy and chemotherapy	HT-29 tumor bearing mice	[63]	
	pH-sensitive poly(beta-amino ester) copolymer NPs	DOX and Cur	<i>i.v.</i> injection	Antiangiogenesis therapy and chemotherapy	SMMC 7721 tumor bearing mice	[64]	
	Captopril-polyethyleneimine conjugated AuNPs	Captopril and siRNA	<i>i.v.</i> injection	Antiangiogenesis and gene therapy	MDA-MB-435 tumor bearing mice	[66]	
	Calcium phosphate NPs	anti-VEGF shRNA and $\gamma$ CDglyTK	Intraperitoneal or intratumoral administration	Antiangiogenic gene therapy and suicide gene therapy	SGC7901 tumor bearing mice	[67]	
VDAs-based cancer starvation therapy	CTX-coupled SNALP-formulated anti-miR-21 oligonucleotides	CTX and anti-miR-21	<i>i.v.</i> or oral administration	Antiangiogenesis therapy and gene therapy	GBM tumor bearing mice	[68]	
	RhoJ antibody modified Au@I NPs	RhoJ antibody	<i>i.v.</i> injection	Antiangiogenesis therapy and radiotherapy	Patient-derived tumor xenografts	[61]	
	AuNPs	anti-VEGF siRNA	Intratumoral injection and laser irritation (655 nm)	Antiangiogenic gene therapy and photothermal therapy	PC-3 tumor bearing mice	[31]	
	Near infrared probe iron oxide NPs	Bevacizumab	<i>i.v.</i> injection	Antiangiogenesis therapy and imaging	4T1 tumor bearing mice	[58]	
	Sorafenib and Ce6 formed carrier-free NPs	Sorafenib and Ce6	<i>i.v.</i> injection and laser irritation (660 nm)	Antiangiogenesis therapy and photodynamic therapy	HSC3 tumor bearing mice	[72]	
	DOX-PLGA-conjugate NPs	Free CA4 and DOX	<i>i.v.</i> injection	Starvation therapy and chemotherapy	Lewis lung carcinoma xenografts and B16F10 tumor bearing mice	[23]	
	LyP-1 coated liposomes	Free Ombrabulin and DOX	<i>i.v.</i> injection	Starvation therapy and chemotherapy	MDA-MB-435 tumor bearing mice	[74]	
	Poly(L-glutamic acid)-g-mPEG NPs	Free CA4P and CDDP	<i>i.v.</i> injection	Starvation therapy and chemotherapy	MDA-MB-435 tumor bearing mice	[75]	
	A15-PGA-CDDP NPs	Free DMXAA and CDDP	<i>i.v.</i> injection	Starvation therapy and chemotherapy	C26 tumor bearing mice	[42]	
	CA4-NPs	CA4	<i>i.v.</i> injection	Starvation therapy	C26 tumor bearing mice	[28]	
	mPEG- <i>b</i> -PHEA-DMXAA conjugate NPs	DMXAA and DOX	<i>i.v.</i> injection	Starvation therapy and chemotherapy	MCF-7 tumor bearing mice	[76]	
	CA4-NPs	CA4 and TPZ	<i>i.v.</i> injection	Starvation therapy and chemotherapy	4T1 tumor bearing mice	[27]	
	CA4-NPs and MMP9-DOX-NPs	CA4 and DOX	<i>i.v.</i> injection	Starvation therapy and chemotherapy	4T1 and C26 tumor bearing mice	[78]	
	Vascular blockade-induced cancer starvation therapy	CREKA modified IONPs and CRKDKC modified iron oxide nanoworms	Two tumor-homing peptide of CREKA and CRKDKC	<i>i.v.</i> injection	Starvation therapy	22Rv1 tumor bearing mice	[88]
		DNA nanorobots	Thrombin	<i>i.v.</i> injection	Starvation therapy	MDA-MB-231 tumor bearing mice	[26]
PVP-modified Mg <sub>2</sub> Si NPs		Mg <sub>2</sub> Si	Intratumoral injection	Starvation therapy	4T1 tumor bearing mice	[11]	
TPZ-MNPs		Mg <sub>2</sub> Si and TPZ	Intratumoral injection	Starvation therapy and hypoxia-activated chemotherapy	4T1 tumor bearing mice	[38]	



GOx-mediated cancer starvation therapy	GOx-MnO <sub>2</sub> @HA NPs	GOx and MnO <sub>2</sub>	Intratumoral injection	Starvation therapy	CT-26 tumor bearing mice	[98]
	Large pore-sized dendritic silica NPs	GOx and Fe <sub>3</sub> O <sub>4</sub> NPs	Intratumoral or <i>i.v.</i> injection	Starvation therapy and oxidation therapy	4T1 and U87 tumor xenografts	[106]
	PEG- <i>b</i> -P(PBEM- <i>co</i> -PEM) NPs	GOx and QM	<i>i.v.</i> injection	Starvation therapy and oxidation therapy	A549 tumor bearing mice	[101]
	Poly(FBMA- <i>co</i> -OEGMA) nanogels	GOx	Intratumoral injection	Starvation therapy and oxidation therapy	C8161 tumor bearing mice	[96]
	Fe <sub>3</sub> C <sub>2</sub> -GOx@MnO <sub>2</sub> NCs	GOx, Fe <sub>3</sub> C <sub>2</sub> and MnO <sub>2</sub>	<i>i.v.</i> injection	Starvation therapy and oxidation therapy	U14 and 4T1 tumor bearing mice	[107]
	GOx-CPO@ZIF-8@NM NPs	GOx and CPO	<i>i.v.</i> injection	Starvation therapy and oxidation therapy	4T1 tumor bearing mice	[109]
	ATP-responsive GOx@ZIF@MPN NPs	GOx and Fe(III)/Fe(II)	Intratumoral injection	Starvation therapy and oxidation therapy	4T1 tumor bearing mice	[108]
	FDMSNs@GOx@HA	GOx and Ferrocene	<i>i.v.</i> injection	Starvation therapy and oxidation therapy	HeLa tumor bearing mouse	[148]
	GOx@PCPT-NR	GOx and CPT prodrug	<i>i.v.</i> injection	Starvation therapy and chemotherapy	A549 tumor bearing mice	[41]
	Mem@GOx@ZIF-8@BDO X) NPs	GOx and BDOX	<i>i.v.</i> injection	Starvation therapy and chemotherapy	4T1 tumor bearing mice	[99]
	MSNs-GOx/PLL/HA	GOx and PTX	<i>i.v.</i> injection	Starvation therapy and chemotherapy	HepG2 tumor bearing mice	[149]
	Yolk-shell tetrasulfide bond bridged dendritic MONs	GOx and AQ4N	Intratumoral injection	Starvation therapy and hypoxia-activated chemotherapy	4T1 tumor bearing mice	[33]
	TGZ@eM NRs	GOx and TPZ	<i>i.v.</i> injection	Starvation therapy and hypoxia-activated chemotherapy	CT26 tumor bearing mice	[13]
	HA-coated CaCO <sub>3</sub> NPs	GOx and TPZ	<i>i.v.</i> injection	Starvation therapy and hypoxia-activated chemotherapy	CT26 tumor bearing mice	[100]
	Liposomes	GOx and AQ4N	Intratumoral injection	Starvation therapy and hypoxia-activated chemotherapy	4T1 tumor bearing mice	[30]
	BCE <sub>TPZ</sub> @(GOx+CAT)	GOx, CAT and TPZ	<i>i.v.</i> injection	Starvation therapy and hypoxia-activated chemotherapy	EMT-6 tumor bearing mice	[94]
	GOx conjugated polymer dots	GOx	Intratumoral injection and laser irritation (460 nm)	Starvation therapy and photodynamic therapy	MCF-7 tumor bearing mice	[115]
	Mem@catalase@GOx@PC N-224 bioreactor	GOx, CAT and TCP	<i>i.v.</i> injection and laser irritation (660 nm)	Starvation therapy and photodynamic therapy	4T1 tumor bearing mice	[44]
	HMSNs	GOx and Ce6	<i>i.v.</i> injection	Starvation therapy and photodynamic therapy	B16F10 metastatic tumor bearing mice	[32]
	Hollow-MnO <sub>2</sub> -GOx-Ce6@CM	GOx, MnO <sub>2</sub> and Ce6	<i>i.v.</i> injection and laser irritation (655 nm)	Starvation therapy and photodynamic therapy	B16F10 tumor bearing mice	[150]
	rMGB	GOx, MnO <sub>2</sub> and Ce6	<i>i.v.</i> injection and laser irradiation (660 nm)	Starvation therapy and photodynamic therapy	4T1 cancer bearing mice	[120]
	PEGylate HA-functionalized PHPBNs	GOx	<i>i.v.</i> injection and NIR laser irritation (808 nm)	Starvation therapy and photothermal therapy	HepG2 tumor bearing mice	[121]
	BSA-directed two-dimensional MnO <sub>2</sub> nanosheet	MnO <sub>2</sub>	<i>i.v.</i> injection and NIR laser irritation (808 nm)	Starvation therapy and photothermal therapy	U87MG tumor bearing mice	[122]
GOx-conjugated silver nanocubes	GOx and Ag ions	Intratumoral injection	Starvation therapy and metal ion therapy	4T1 tumor bearing mice	[113]	
HMONs	L-Arg and GOx	Intratumoral injection	Starvation therapy and gas therapy	U87MG tumor bearing mice	[46]	
CMSNs	GOx and anti-PD-1	<i>i.v.</i> injection	Starvation therapy and immunotherapy	B16F10 tumor bearing mice	[47]	
Fe <sub>3</sub> O <sub>4</sub> @PPy@GOx NCs	GOx, Fe <sub>3</sub> O <sub>4</sub> NPs and PPy	<i>i.v.</i> injection and NIR laser irradiation (808 or 1064 nm)	Starvation therapy, oxidation therapy and photodynamic therapy	4T1 tumor bearing mice	[45]	
CPT@MOF(Fe)-GOx	GOx, Fe <sup>3+</sup> and CPT	Intratumoral injection	Starvation therapy, oxidation therapy and chemotherapy	HeLa tumor bearing mice	[151]	
MGH nanoamplifier	GOx and MIL-100	<i>i.v.</i> injection, NIR laser irradiation (808 nm)	Starvation therapy, oxidation therapy, photothermal therapy and imaging	4T1 tumor bearing mice	[110]	
Other strategies for cancer starvation therapy	HDL-AuNPs	HDL	<i>i.v.</i> injection	Starvation therapy	B-cell lymphoma xenografts	[39]
	HDL-AuNPs	HDL	<i>i.v.</i> injection	Starvation therapy and immunotherapy	LLC tumor bearing mice and melanoma metastatic lung colonization mice model	[140]
	CHC-PZM@HA	CHC and PZM	<i>i.v.</i> injection, laser irradiation (660 nm)	Starvation therapy and photodynamic therapy	CT26 tumor bearing mice	[40]
	Mn-D@BPFe-A NPs	DOX, Fe <sup>3+</sup>		Starvation therapy, chemotherapy and photodynamic therapy	HepG2 tumor bearing mice	[141]

However, most innovations in this field are still in their infancy, with underlying challenges regarding clinical translation that need to be assessed in detail.

For example, the biosafety of these nanomaterials is still significantly concerned, especially for the non-biodegradable formulations. Although the

biosafety assessment of these materials could be systematically evaluated through animal models, long-term internal metabolic behaviors and related toxicity should be thoroughly investigated before clinical application. Another major concern is the aggravating hypoxia level that may accelerate the tumor invasion and metastasis in the progress of tumor starvation therapy. Detailed studies should be performed to confirm whether cancer starvation therapy could turn on the tumor metastasis switch by elevating the hypoxic TME, which would also help to develop new combination strategies for offering synergistic effects. Moreover, in addition to elevating the hypoxia level, these cancer starvation-based methods could also increase the intratumoral acidity and/or promoting the intracellular oxidative stress. It remains unknown how these changes influence the local and systemic immune responses. The advances in cancer immunotherapy would offer new insights and perspectives for further evolving cancer starvation-based treatments [144].

#### 4. Abbreviations

**Table 2.** List of abbreviations

·OH	Hydroxyl radical	DMXAA	5,6-dimethylxanthenone-4-acetic acid
<sup>1</sup> O <sub>2</sub>	Singlet oxygen	DOX	Doxorubicin
2D	Two-dimensional	ECs	Endothelial cells
4T1	Mice breast tumor cell line	EEPT	Enzyme-enhanced phototherapy
22Rv1	Human prostate cancer cell line	eM	Erythrocyte membrane
A431	Human epidermoid carcinoma cell line	EMT-6	Mouse mammary cancer cell line
A549	Human lung cancer cell line	EPR	Enhanced permeability and retention
Ag	Silver	FDA	Food and Drug Administration
AIA	Angiogenesis inhibiting agent	FDMSNs	Ferrocene-functionalized dendritic mesoporous silica nanoparticles
anti-PD-1	Programmed cell death protein 1 antibody	GBM	Human glioblastoma cell line
anti-PD-L1	Programmed cell death ligand 1 antibody	GO	Graphene oxide
AQ4N	Banaxantrone dihydrochloride	GOx	Glucose oxidase
AXT	Axitinib	GSH	Glutathione
ATP	Adenosine triphosphate	H <sub>2</sub> O <sub>2</sub>	Hydrogen peroxide
Au NP	Gold nanoparticle	HA	Hyaluronic acid
B16F10	Mouse melanoma cell line	HAP	Hypoxia-activated prodrug
BDOX	H <sub>2</sub> O <sub>2</sub> -sensitive doxorubicin prodrug	HDL	High density lipoprotein
BPEI	Branched polyethylenimine	HFR	Heparin-folic acid-retinoic acid conjugate
BSA	Bovine serum albumin	HMON	Hollow mesoporous organosilica nanoparticle
BCE	PEG- <i>b</i> -PHEMA crosslinked CPZ loaded BSA and CAT/GOx nanoclustered enzymes	H22	Mouse hepatocellular carcinoma cell line
C26	Murine colon cancer cell line	HepG2	Human liver cancer cell line
C8161	Human melanoma cell line	HSC3	Human oral squamous carcinoma cell line
CT26	Mouse colon cancer cell line	HSP	Heat shock protein
CA4	Combretastatin A4	HT-29	Mouse colon tumor cell line
CA4P	Combretastatin A4 disodium phosphate	ICG	Indocyanine green
CA4-NPs	Poly(L-glutamic acid)-CA4 conjugate nanoparticles	ICB	Immune checkpoint blockade
CDDP	Cisplatin	iNGR-NP	iNGR-modified PEG-PLGA nanoparticle
Ce6	Chlorin e6	iNOS	NO synthase enzyme
CHC	<i>α</i> -cyano-4-hydroxycinnamate	IONP	Iron oxide nanoparticle
CM	Cell membrane	<i>i.v.</i>	Intravenous injection
CMSNs	Cancer cell membrane coated mesoporous silica nanoparticles	LyP-1	Phage-displayed cyclic peptide
CPNP	Calcium phosphate nanoparticle	LLC	Lewis lung carcinoma cell line
CPO	Chloroperoxidase	MCF-7	Human breast cancer cell line
CPPO	Bis[2,4,5-trichloro-6-(pentyloxycarbonyl)phenyl]oxalate	MCT1	Monocarboxylate transporter 1
CPT	Camptothecin	MDA-MB-435	Human breast cancer cell line
CST	Celastrol	MDA-MB-231	Human breast cancer cell line
CTX	Chlorotoxin	MDR	Multidrug resistance
Cur	Curcumin	MDSCs	Myeloid-derived suppressor cells
DDS	Drug delivery system	Mg <sub>2</sub> Si	Magnesium silicide
DCs	Dendritic cells	MGP	GOx and MnCO coloaded poly(lactic-co-glycolic acid) nanoparticles
		MIL-100	Ferric ions contained metal organic framework
		MGH	GOx loaded MIL-100 with polydopaminemodified hyaluronic acid coating
		MMC	Mitomycin C
		MMP	Matrix metalloproteinase
		MnO <sub>2</sub>	Manganese dioxide
		M-NS	BSA-directed two-dimensional MnO <sub>2</sub> nanosheet
		MOF	Metal-organic framework
		MOST	Multispectral optoacoustic tomography
		MPN	Metal polyphenol network
		MSN	Mesoporous silica nanoparticle
		MTX	Methotrexate
		nano-DOA	Nano-deoxygenation agent
		NC	Nanocatalyst
		NIR	Near-infrared
		NM	Neutrophil membrane
		NO	Nitric oxide
		NP	Nanoparticle
		NR	Nanoreactor
		O <sub>2</sub>	Oxygen
		OCI-	Hypochlorite ion
		OSCC	Oral squamous carcinoma cell line
		PC-3	Human prostate cancer cell line
		Pdot	Polymer dot
		PDT	Photodynamic therapy
		PFC	Perfluorocarbon
		PLA	Poly-L-arginine
		PLL	poly(L-lysine)
		PLGA	Poly(lactic-co-glycolic acid)
		PEG	Poly(ethylene glycol)
		PEG- <i>b</i> -PHEMA	poly(ethylene glycol)- <i>block</i> -poly(2-hydroxyethyl methacrylate)
		PLG-g-mPEG	Poly(L-glutamic acid)-g-methoxy poly(ethylene glycol)

PPy	Polypyrrole
PTT	Photothermal therapy
PTX	Paclitaxel
PVP	Polyvinyl pyrrolidone
PZM	Porous Zr (IV)-based porphyrinic metal-organic framework
RA	Retinoic acid
RBC	Red blood cell
RGD	Arginine-glycine-aspartic acid
rMGB	Biomimetic hybrid nanozyme with a GOx/MnO <sub>2</sub> /BSA-Ce6 core and red blood cell membrane coating
ROS	Reactive oxygen species
SCC7	Murine squamous cell carcinoma cell line
SGC7901	Gastric cancer cell line
shVEGF	VEGF-targeted small hairpin RNA
SiO <sub>2</sub>	Silicon dioxide
siRNA	Small interfering RNA
SMMC 7721	Human liver tumor cell line
SR-B1	Scavenger receptor type B-1
SW620	Human Caucasian colon adenocarcinoma cell line
TACE	Transarterial chemoembolization
TAF	Tumor angiogenesis factor
TCPP	Tetrakis (4-carboxyphenyl) porphyrin
THP	Tumor-homing peptide
TME	Tumor microenvironment
TPZ	Tirapazamine
UV	Ultraviolet
VDA	Vascular disrupting agent
VEGF	Vascular endothelial growth factor
U14	Mouse cervical subcutaneous cancer cell line
U87	Human glioblastoma cell line
U87MG	Human glioblastoma cell line
Vx2	Rabbit carcinoma cell line
yCDglyTK	Fusion suicide gene
ZIF-8	Zeolitic imidazolate framework-8
$\alpha_4\beta_3$ -Dxtl-PD NP	$\alpha_4\beta_3$ -integrin targeted perfluorocarbon nanoparticle

## Acknowledgements

This work was supported by the the start-up package at UCLA (to Z.G.), the National Natural Science Foundation of China (NSFC 51773199 to S.Y.) and the start-up fund from Hangzhou Normal University (4095C5021920450 to S.Y.).

## Competing Interests

The authors have declared that no competing interest exists.

## References

- Bray F, Ferlay J, Soerjomataram I, Siegel RL, Torre LA, Jemal A. Global cancer statistics 2018: GLOBOCAN estimates of incidence and mortality worldwide for 36 cancers in 185 countries. *CA-Cancer J Clin.* 2018; 68: 394-424.
- Siegel RL, Miller KD, Jemal A. Cancer statistics, 2018. *CA-Cancer J Clin.* 2018; 68: 7-30.
- Selwan EM, Finicle BT, Kim SM, Edinger AL. Attacking the supply wagons to starve cancer cells to death. *FEBS Lett.* 2016; 590: 885-907.
- Fu LH, Qi C, Lin J, Huang P. Catalytic chemistry of glucose oxidase in cancer diagnosis and treatment. *Chem Soc Rev.* 2018; 47: 6454-72.
- Maddocks OD, Berkers CR, Mason SM, Zheng L, Blyth K, Gottlieb E, et al. Serine starvation induces stress and p53-dependent metabolic remodelling in cancer cells. *Nature.* 2013; 493: 542-6.
- Rafii S, Lyden D, Benezra R, Hattori K, Heissig B. Vascular and haematopoietic stem cells: novel targets for anti-angiogenesis therapy? *Nat Rev Cancer.* 2002; 2: 826-35.
- Shojaei F. Anti-angiogenesis therapy in cancer: current challenges and future perspectives. *Cancer Lett.* 2012; 320: 130-7.
- Tozer GM, Kanthou C, Baguley BC. Disrupting tumour blood vessels. *Nat Rev Cancer.* 2005; 5: 423.
- Chase DM, Chaplin DJ, Monk BJ. The development and use of vascular targeted therapy in ovarian cancer. *Gynecol Oncol.* 2017; 145: 393-406.

- Lin WH, Yeh SH, Yeh KH, Chen KW, Cheng YW, Su TH, et al. Hypoxia-activated cytotoxic agent tirapazamine enhances hepatic artery ligation-induced killing of liver tumor in HBx transgenic mice. *PNAS.* 2016; 113: 11937-42.
- Zhang C, Ni D, Liu Y, Yao H, Bu W, Shi J. Magnesium silicide nanoparticles as a deoxygenation agent for cancer starvation therapy. *Nat Nanotechnol.* 2017; 12: 378-86.
- Feron O. Pyruvate into lactate and back: from the Warburg effect to symbiotic energy fuel exchange in cancer cells. *Radiother Oncol.* 2009; 92: 329-33.
- Zhang L, Wang Z, Zhang Y, Cao F, Dong K, Ren J, et al. Erythrocyte Membrane Cloaked Metal-Organic Framework Nanoparticle as Biomimetic Nanoreactor for Starvation-Activated Colon Cancer Therapy. *ACS Nano.* 2018; 12: 10201-11.
- Bergers G, Hanahan D. Modes of resistance to anti-angiogenic therapy. *Nat Rev Cancer.* 2008; 8: 592-603.
- Hollebecque A, Massard C, Soria JC. Vascular disrupting agents: a delicate balance between efficacy and side effects. *Curr Opin Oncol.* 2012; 24: 305-15.
- De Bock K, Mazzone M, Carmeliet P. Antiangiogenic therapy, hypoxia, and metastasis: risky liaisons, or not? *Nat Rev Clin Oncol.* 2011; 8: 393-404.
- Chung BL, Toth MJ, Kamaly N, Sei YJ, Becraft J, Mulder WJ, et al. Nanomedicines for Endothelial Disorders. *Nano Today.* 2015; 10: 759-76.
- Yu S, He C, Chen X. Injectable Hydrogels as Unique Platforms for Local Chemotherapeutics-Based Combination Antitumor Therapy. *Macromol Biosci.* 2018; 18: e1800240.
- Shi J, Kantoff PW, Wooster R, Farokhzad OC. Cancer nanomedicine: progress, challenges and opportunities. *Nat Rev Cancer.* 2017; 17: 20-37.
- Fan W, Yung B, Huang P, Chen X. Nanotechnology for Multimodal Synergistic Cancer Therapy. *Chem Rev.* 2017; 117: 13566-638.
- Lu Y, Aimeetti AA, Langer R, Gu Z. Bioresponsive materials. *Nat Rev Mater.* 2016; 1: 16075-81.
- Sun W, Hu Q, Ji W, Wright G, Gu Z. Leveraging Physiology for Precision Drug Delivery. *Physiol Rev.* 2016; 97: 189-225.
- Sengupta S, Eavarone D, Capila I, Zhao G, Watson N, Kiziltepe T, et al. Temporal targeting of tumour cells and neovasculature with a nanoscale delivery system. *Nature.* 2005; 436: 568-72.
- Park IK, Tran TH, Oh IH, Kim YJ, Cho KJ, Huh KM, et al. Ternary biomolecular nanoparticles for targeting of cancer cells and anti-angiogenesis. *Eur J Pharm Sci.* 2010; 41: 148-55.
- Zhang E, Xing R, Liu S, Li K, Qin Y, Yu H, et al. Vascular targeted chitosan-derived nanoparticles as docetaxel carriers for gastric cancer therapy. *Int J Biol Macromol.* 2019; 126: 662-72.
- Li S, Jiang Q, Liu S, Zhang Y, Tian Y, Song C, et al. A DNA nanorobot functions as a cancer therapeutic in response to a molecular trigger *in vivo*. *Nat Biotechnol.* 2018; 36: 258.
- Yang S, Tang Z, Hu C, Zhang D, Shen N, Yu H, et al. Selectively Potentiating Hypoxia Levels by Combretastatin A4 Nanomedicine: Toward Highly Enhanced Hypoxia-Activated Prodrug Tirapazamine Therapy for Metastatic Tumors. *Adv Mater.* 2019; e1805955.
- Liu TZ, Zhang DW, Song WT, Tang ZH, Zhu JM, Ma ZM, et al. A poly(L-glutamic acid)-combretastatin A4 conjugate for solid tumor therapy: Markedly improved therapeutic efficiency through its low tissue penetration in solid tumor. *Acta Biomater.* 2017; 53: 179-89.
- He WY, Zheng X, Zhao Q, Duan LJ, Lv Q, Gao GH, et al. pH-Triggered Charge-Reversal Polyurethane Micelles for Controlled Release of Doxorubicin. *Macromol Biosci.* 2016; 16: 925-35.
- Zhang R, Feng L, Dong Z, Wang L, Liang C, Chen J, et al. Glucose & oxygen exhausting liposomes for combined cancer starvation and hypoxia-activated therapy. *Biomaterials.* 2018; 162: 123-31.
- Son S, Kim N, You DG, Yoon HY, Yhee JY, Kim K, et al. Antitumor therapeutic application of self-assembled RNAi-AuNP nanoconstructs: Combination of VEGF-RNAi and photothermal ablation. *Theranostics.* 2017; 7: 9-22.
- Yu Z, Zhou P, Pan W, Li N, Tang B. A biomimetic nanoreactor for synergistic chemiexcited photodynamic therapy and starvation therapy against tumor metastasis. *Nat Commun.* 2018; 9: 5044.
- Yang Y, Lu Y, Abbaraju PL, Azimi I, Lei C, Tang J, et al. Stepwise Degradable Nanocarriers Enabled Cascade Delivery for Synergistic Cancer Therapy. *Adv Funct Mater.* 2018; 28: 1800706.
- Prasad P, Shuhendler A, Cai P, Rauth AM, Wu XY. Doxorubicin and mitomycin C co-loaded polymer-lipid hybrid nanoparticles inhibit growth of sensitive and multidrug resistant human mammary tumor xenografts. *Cancer Lett.* 2013; 334: 263-73.
- Jing L, Qu H, Wu D, Zhu C, Yang Y, Jin X, et al. Platelet-camouflaged nanococktail: Simultaneous inhibition of drug-resistant tumor growth and metastasis via a cancer cells and tumor vasculature dual-targeting strategy. *Theranostics.* 2018; 8: 2683-95.

36. Mukherjee S, Patra CR. Therapeutic application of anti-angiogenic nanomaterials in cancers. *Nanoscale*. 2016; 8: 12444-70.
37. Laakkonen P, Porkka K, Hoffman JA, Ruoslahti E. A tumor-homing peptide with a targeting specificity related to lymphatic vessels. *Nat Med*. 2002; 8: 751-5.
38. Chen C, Su W, Liu Y, Zhang J, Zuo C, Yao Z, et al. Artificial anaerobic cell dormancy for tumor gaseous microenvironment regulation therapy. *Biomaterials*. 2019; 200: 48-55.
39. Yang S, Damiano MG, Zhang H, Tripathy S, Luthi AJ, Rink JS, et al. Biomimetic, synthetic HDL nanostructures for lymphoma. *PNAS*. 2013; 110: 2511-6.
40. Chen Z-X, Liu M-D, Zhang M-K, Wang S-B, Xu L, Li C-X, et al. Interfering with Lactate-Fueled Respiration for Enhanced Photodynamic Tumor Therapy by a Porphyrinic MOF Nanoplatfrom. *Adv Funct Mater*. 2018; 28: 1803498.
41. Li J, Li Y, Wang Y, Ke W, Chen W, Wang W, et al. Polymer Prodrug-Based Nanoreactors Activated by Tumor Acidity for Orchestrated Oxidation/Chemotherapy. *Nano Lett*. 2017; 17: 6983-90.
42. Song W, Tang Z, Zhang D, Li M, Gu J, Chen X. A cooperative polymeric platform for tumor-targeted drug delivery. *Chem Sci*. 2016; 7: 728-36.
43. Chen Y, Gu H, Zhang DS, Li F, Liu T, Xia W. Highly effective inhibition of lung cancer growth and metastasis by systemic delivery of siRNA via multimodal mesoporous silica-based nanocarrier. *Biomaterials*. 2014; 35: 10058-69.
44. Li SY, Cheng H, Xie BR, Qiu WX, Zeng JY, Li CX, et al. Cancer Cell Membrane Camouflaged Cascade Bioreactor for Cancer Targeted Starvation and Photodynamic Therapy. *ACS Nano*. 2017; 11: 7006-18.
45. Feng W, Han X, Wang R, Gao X, Hu P, Yue W, et al. Nanocatalysts-Augmented and Photothermal-Enhanced Tumor-Specific Sequential Nanocatalytic Therapy in Both NIR-I and NIR-II Biowindows. *Adv Mater*. 2019; 31: e1805919.
46. Fan W, Lu N, Huang P, Liu Y, Yang Z, Wang S, et al. Glucose-Responsive Sequential Generation of Hydrogen Peroxide and Nitric Oxide for Synergistic Cancer Starving-Like/Gas Therapy. *Angew Chem Int Ed*. 2017; 56: 1229-33.
47. Xie W, Deng WW, Zan M, Rao L, Yu GT, Zhu DM, et al. Cancer Cell Membrane Camouflaged Nanoparticles to Realize Starvation Therapy Together with Checkpoint Blockades for Enhancing Cancer Therapy. *ACS Nano*. 2019; 13: 2849-57.
48. Carmeliet P, Jain RK. Angiogenesis in cancer and other diseases. *Nature*. 2000; 407: 249-57.
49. Wang JC, Sun X, Ma Q, Fu GF, Cong LL, Zhang H, et al. Metformin's antitumor and anti-angiogenic activities are mediated by skewing macrophage polarization. *J Cell Mol Med*. 2018.
50. Jain RK. Antiangiogenesis strategies revisited: from starving tumors to alleviating hypoxia. *Cancer cell*. 2014; 26: 605-22.
51. Ellis LM, Hicklin DJ. VEGF-targeted therapy: mechanisms of anti-tumor activity. *Nat Rev Cancer*. 2008; 8: 579-91.
52. Maeda H. The enhanced permeability and retention (EPR) effect in tumor vasculature: the key role of tumor-selective macromolecular drug targeting. *Adv Enzyme Regul* 2001; 41: 189-207.
53. Sui H, Zhao J, Zhou L, Wen H, Deng W, Li C, et al. Tanshinone IIA inhibits beta-catenin/VEGF-mediated angiogenesis by targeting TGF-beta1 in normoxic and HIF-1alpha in hypoxic microenvironments in human colorectal cancer. *Cancer Lett*. 2017; 403: 86-97.
54. Pan D, Schmieder AH, Wang K, Yang X, Senpan A, Cui G, et al. Anti-angiogenesis therapy in the Vx2 rabbit cancer model with a lipase-cleavable Sn 2 taxane phospholipid prodrug using alpha(v)beta(3)-targeted theranostic nanoparticles. *Theranostics*. 2014; 4: 565-78.
55. Esser AK, Schmieder AH, Ross MH, Xiang J, Su X, Cui G, et al. Dual-therapy with alphavbeta3-targeted Sn2 lipase-labile fumagillin-prodrug nanoparticles and zoledronic acid in the Vx2 rabbit tumor model. *Nanomedicine*. 2016; 12: 201-11.
56. Kang T, Gao X, Hu Q, Jiang D, Feng X, Zhang X, et al. iNGR-modified PEG-PLGA nanoparticles that recognize tumor vasculature and penetrate gliomas. *Biomaterials*. 2014; 35: 4319-32.
57. Eldar-Boock A, Miller K, Sanchis J, Lupu R, Vicent MJ, Satchi-Fainaro R. Integrin-assisted drug delivery of nano-scaled polymer therapeutics bearing paclitaxel. *Biomaterials*. 2011; 32: 3862-74.
58. Lin R, Huang J, Wang L, Li Y, Lipowska M, Wu H, et al. Bevacizumab and near infrared probe conjugated iron oxide nanoparticles for vascular endothelial growth factor targeted MR and optical imaging. *Biomater Sci*. 2018; 6: 1517-25.
59. Hu Q, Sun W, Wang C, Gu Z. Recent advances of cocktail chemotherapy by combination drug delivery systems. *Adv Drug Deliv Rev*. 2016; 98: 19-34.
60. Hu CM, Zhang L. Nanoparticle-based combination therapy toward overcoming drug resistance in cancer. *Biochem Pharmacol*. 2012; 83: 1104-11.
61. Liu S, Li H, Xia L, Xu P, Ding Y, Huo D, et al. Anti-RhoJ antibody functionalized Au@I nanoparticles as CT-guided tumor vessel-targeting radiosensitizers in patient-derived tumor xenograft model. *Biomaterials*. 2017; 141: 1-12.
62. Abbasi MM, Monfaredan A, Hamishehkar H, Seidi K, Jahanban-Esfahlan R. Novel DOX-MTX Nanoparticles Improve Oral SCC Clinical Outcome by Down Regulation of Lymph Dissemination Factor VEGF-C Expression *in vivo*: Oral and IV Modalities. *Asian Pac J Cancer Prev*. 2014; 15: 6227-32.
63. Shi L, Hu Y, Lin A, Ma C, Zhang C, Su Y, et al. Matrix Metalloproteinase Responsive Nanoparticles for Synergistic Treatment of Colorectal Cancer via Simultaneous Anti-Angiogenesis and Chemotherapy. *Bioconjug Chem*. 2016; 27: 2943-53.
64. Zhang J, Li J, Shi Z, Yang Y, Xie X, Lee SM, et al. pH-sensitive polymeric nanoparticles for co-delivery of doxorubicin and curcumin to treat cancer via enhanced pro-apoptotic and anti-angiogenic activities. *Acta Biomater*. 2017; 58: 349-64.
65. Kim MG, Jo SD, Yhee JY, Lee BS, Lee SJ, Park SG, et al. Synergistic anti-tumor effects of bevacizumab and tumor targeted polymerized VEGF siRNA nanoparticles. *Biochem Biophys Res Commun*. 2017; 489: 35-41.
66. Li M, Li Y, Huang X, Lu X. Captopril-polyethyleneimine conjugate modified gold nanoparticles for co-delivery of drug and gene in anti-angiogenesis breast cancer therapy. *J Biomater Sci Polym Ed*. 2015; 26: 813-27.
67. Liu T, Ye L, He Y, Chen X, Peng J, Zhang X, et al. Combination gene therapy using VEGF-shRNA and fusion suicide gene yCDglyTK inhibits gastric carcinoma growth. *Exp Mol Pathol*. 2011; 91: 745-52.
68. Costa PM, Cardoso AL, Custodia C, Cunha P, Pereira de Almeida L, Pedrosa de Lima MC. MiRNA-21 silencing mediated by tumor-targeted nanoparticles combined with sunitinib: A new multimodal gene therapy approach for glioblastoma. *J Control Release*. 2015; 207: 31-9.
69. Cheng L, Wang C, Feng L, Yang K, Liu Z. Functional nanomaterials for phototherapies of cancer. *Chem Rev*. 2014; 114: 10869-939.
70. Qian C, Yu J, Chen Y, Hu Q, Xiao X, Sun W, et al. Light-Activated Hypoxia-Responsive Nanocarriers for Enhanced Anticancer Therapy. *Adv Mater*. 2016; 28: 3313-20.
71. Tang Z, Zhang H, Liu Y, Ni D, Zhang H, Zhang J, et al. Antiferromagnetic Pyrite as the Tumor Microenvironment-Mediated Nanoplatfrom for Self-Enhanced Tumor Imaging and Therapy. *Adv Mater*. 2017; 29.
72. Wei Z, Liang P, Xie J, Song C, Tang C, Wang Y, et al. Carrier-free nano-integrated strategy for synergetic cancer anti-angiogenic therapy and phototherapy. *Chem Sci*. 2019; 10: 2778-84.
73. Cooney MM, van Heeckeren W, Bhakta S, Ortiz J, Remick SC. Drug insight: vascular disrupting agents and angiogenesis—novel approaches for drug delivery. *Nat Clin Pract Oncol*. 2006; 3: 682-92.
74. Lin KY, Kwon EJ, Lo JH, Bhatia SN. Drug-induced amplification of nanoparticle targeting to tumors. *Nano Today*. 2014; 9: 550-9.
75. Song W, Tang Z, Zhang D, Yu H, Chen X. Coadministration of Vascular Disrupting Agents and Nanomedicines to Eradicate Tumors from Peripheral and Central Regions. *Small*. 2015; 11: 3755-61.
76. Lv S, Tang Z, Song W, Zhang D, Li M, Liu H, et al. Inhibiting Solid Tumor Growth *In vivo* by Non-Tumor-Penetrating Nanomedicine. *Small*. 2017; 13.
77. Yu S, Wei S, Liu L, Qi D, Wang J, Chen G, et al. Enhanced local cancer therapy using a CA4P and CDDP co-loaded polypeptide gel depot. *Biomater Sci*. 2019; 7: 860-6.
78. Jiang J, Shen N, Ci T, Tang Z, Gu Z, Li G, et al. Combretastatin A4 Nanodrug-Induced MMP9 Amplification Boosts Tumor-Selective Release of Doxorubicin Prodrug. *Adv Mater*. 2019; e1904278.
79. Nichols JW, Bae YH. EPR: Evidence and fallacy. *J Control Release*. 2014; 190: 451-64.
80. Kanapathipillai M, Brock A, Ingber DE. Nanoparticle targeting of anti-cancer drugs that alter intracellular signaling or influence the tumor microenvironment. *Adv Drug Deliv Rev*. 2014; 79-80: 107-18.
81. Fogal V, Zhang L, Krajewski S, Ruoslahti E. Mitochondrial/cell-surface protein p32/gC1qR as a molecular target in tumor cells and tumor stroma. *Cancer Res*. 2008; 68: 7210-8.
82. Pouyssegur J, Dayan F, Mazure NM. Hypoxia signalling in cancer and approaches to enforce tumour regression. *Nature*. 2006; 441: 437-43.
83. Yu J, Zhang Y, Hu X, Wright G, Gu Z. Hypoxia-Sensitive Materials for Biomedical Applications. *Ann Biomed Eng*. 2016; 44: 1931-45.
84. Brown JM, Wilson WR. Exploiting tumour hypoxia in cancer treatment. *Nat Rev Cancer*. 2004; 4: 437-47.

85. Rischin D, Hicks RJ, Fisher R, Binns D, Corry J, Porceddu S, et al. Prognostic Significance of  $[^{18}\text{F}]$ -Misonidazole Positron Emission Tomography-Detected Tumor Hypoxia in Patients With Advanced Head and Neck Cancer Randomly Assigned to Chemoradiation With or Without Tirapazamine: A Substudy of Trans-Tasman Radiation Oncology Group Study 98.02. *J Clin Oncol*. 2006; 24: 2098-104.
86. Ruoslahti E. Peptides as targeting elements and tissue penetration devices for nanoparticles. *Adv Mater*. 2012; 24: 3747-56.
87. Simberg D, Duza T, Park JH, Essler M, Pilch J, Zhang L, et al. Biomimetic amplification of nanoparticle homing to tumors. *PNAS*. 2007; 104: 932-6.
88. Agemy L, Sugahara KN, Kotamraju VR, Gujrati K, Girard OM, Kono Y, et al. Nanoparticle-induced vascular blockade in human prostate cancer. *Blood*. 2010; 116: 2847-56.
89. Semenza GL. Life with oxygen. *Science*. 2007; 318: 62-4.
90. Hamanaka RB, Chandel NS. Targeting glucose metabolism for cancer therapy. *J Exp Med*. 2012; 209: 211-5.
91. Wang C, Ye Y, Hochu GM, Sadeghifar H, Gu Z. Enhanced Cancer Immunotherapy by Microneedle Patch-Assisted Delivery of Anti-PD1 Antibody. *Nano Lett*. 2016; 16: 2334-40.
92. Trachootham D, Alexandre J, Huang P. Targeting cancer cells by ROS-mediated mechanisms: a radical therapeutic approach? *Nat Rev Drug Discov*. 2009; 8: 579-91.
93. Reuter S, Gupta SC, Chaturvedi MM, Aggarwal BB. Oxidative stress, inflammation, and cancer: how are they linked? *Free Radic Biol Med*. 2010; 49: 1603-16.
94. Ma Y, Zhao Y, Bejjanki NK, Tang X, Jiang W, Dou J, et al. Nanoclustered Cascaded Enzymes for Targeted Tumor Starvation and Deoxygenation-Activated Chemotherapy without Systemic Toxicity. *ACS Nano*. 2019; 13: 8890-902.
95. Son YO, Kook SH, Jang YS, Shi X, Lee JC. Critical role of poly(ADP-ribose) polymerase-1 in modulating the mode of cell death caused by continuous oxidative stress. *J Cell Biochem*. 2009; 108: 989-97.
96. Zhao W, Hu J, Gao W. Glucose Oxidase-Polymer Nanogels for Synergistic Cancer-Starving and Oxidation Therapy. *ACS Appl Mater Interfaces*. 2017; 9: 23528-35.
97. Dinda S, Sarkar S, Das PK. Glucose oxidase mediated targeted cancer-starving therapy by biotinylated self-assembled vesicles. *Chem Commun*. 2018; 54: 9929-32.
98. Zhang YH, Qiu WX, Zhang M, Zhang L, Zhang XZ.  $\text{MnO}_2$  Motor: A Prospective Cancer-Starving Therapy Promoter. *ACS Appl Mater Interfaces*. 2018; 10: 15030-9.
99. Cheng H, Jiang XY, Zheng RR, Zuo SJ, Zhao LP, Fan GL, et al. A biomimetic cascade nanoreactor for tumor targeted starvation therapy-amplified chemotherapy. *Biomaterials*. 2019; 195: 75-85.
100. Zhang MK, Li CX, Wang SB, Liu T, Song XL, Yang XQ, et al. Tumor Starvation Induced Spatiotemporal Control over Chemotherapy for Synergistic Therapy. *Small*. 2018; 14: e1803602.
101. Li J, Dirisala A, Ge Z, Wang Y, Yin W, Ke W, et al. Therapeutic Vesicular Nanoreactors with Tumor-Specific Activation and Self-Destruction for Synergistic Tumor Ablation. *Angew Chem Int Ed*. 2017; 56: 14025-30.
102. Tang Z, Liu Y, He M, Bu W. Chemodynamic Therapy: Tumour Microenvironment-Mediated Fenton and Fenton-like Reactions. *Angew Chem Int Ed*. 2019; 58: 946-56.
103. Gao L, Zhuang J, Nie L, Zhang J, Zhang Y, Gu N, et al. Intrinsic peroxidase-like activity of ferromagnetic nanoparticles. *Nat Nanotechnol*. 2007; 2: 577-83.
104. Chen Z, Yin JJ, Zhou YT, Zhang Y, Song L, Song M, et al. Dual enzyme-like activities of iron oxide nanoparticles and their implication for diminishing cytotoxicity. *ACS Nano*. 2012; 6: 4001-12.
105. Zhang X-Y, Elfarra AA. Potential roles of myeloperoxidase and hypochlorous acid in metabolism and toxicity of alkene hydrocarbons and drug molecules containing olefinic moieties. *Expert Opin Drug Metab Toxicol*. 2017; 13: 513-24.
106. Huo M, Wang L, Chen Y, Shi J. Tumor-selective catalytic nanomedicine by nanocatalyst delivery. *Nat Commun*. 2017; 8: 357.
107. Feng L, Xie R, Wang C, Gai S, He F, Yang D, et al. Magnetic Targeting, Tumor Microenvironment-Responsive Intelligent Nanocatalysts for Enhanced Tumor Ablation. *ACS Nano*. 2018; 12: 11000-12.
108. Zhang L, Wan SS, Li CX, Xu L, Cheng H, Zhang XZ. An Adenosine Triphosphate-Responsive Autocatalytic Fenton Nanoparticle for Tumor Ablation with Self-Supplied  $\text{H}_2\text{O}_2$  and Acceleration of  $\text{Fe(III)}/\text{Fe(II)}$  Conversion. *Nano Lett*. 2018; 18: 7609-18.
109. Zhang C, Zhang L, Wu W, Gao F, Li RQ, Song W, et al. Artificial Super Neutrophils for Inflammation Targeting and  $\text{HClO}$  Generation against Tumors and Infections. *Adv Mater*. 2019; e1901179.
110. Zhang Y, Lin L, Liu L, Liu F, Sheng S, Tian H, et al. Positive feedback nanoamplifier responded to tumor microenvironments for self-enhanced tumor imaging and therapy. *Biomaterials*. 2019; 216: 119255.
111. Soenen SJ, Parak WJ, Rejman J, Manshian B. (Intra)Cellular Stability of Inorganic Nanoparticles: Effects on Cytotoxicity, Particle Functionality, and Biomedical Applications. *Chem Rev*. 2015; 115: 2109-35.
112. Gurunathan S, Han JW, Eppakayala V, Jayaraj M, Kim J-H. Cytotoxicity of biologically synthesized silver nanoparticles in MDA-MB-231 human breast cancer cells. *Biomed Res Int*. 2013; 2013: 535796-.
113. Zhang Y, Yang Y, Jiang S, Li F, Lin J, Wang T, et al. Degradable silver-based nanopatform for synergistic cancer starving-like/metal ion therapy. *Mater Horiz*. 2019; 6: 169-75.
114. Dai Y, Cheng S, Wang Z, Zhang R, Yang Z, Wang J, et al. Hypochlorous Acid Promoted Platinum Drug Chemotherapy by Myeloperoxidase-Encapsulated Therapeutic Metal Phenolic Nanoparticles. *ACS Nano*. 2018; 12: 455-63.
115. Chang K, Liu Z, Fang X, Chen H, Men X, Yuan Y, et al. Enhanced Phototherapy by Nanoparticle-Enzyme via Generation and Photolysis of Hydrogen Peroxide. *Nano Lett*. 2017; 17: 4323-9.
116. Celli JP, Spring BQ, Rizvi I, Evans CL, Samkoe KS, Verma S, et al. Imaging and photodynamic therapy: mechanisms, monitoring, and optimization. *Chem Rev*. 2010; 110: 2795-838.
117. Wang W, Moriyama LT, Bagnato VS. Photodynamic therapy induced vascular damage: an overview of experimental PDT. *Laser Phys Lett*. 2013; 10: 023001.
118. Liu Y, Jiang Y, Zhang M, Tang Z, He M, Bu W. Modulating Hypoxia via Nanomaterials Chemistry for Efficient Treatment of Solid Tumors. *Acc Chem Res*. 2018; 51: 2502-11.
119. Fan W, Huang P, Chen X. Overcoming the Achilles' heel of photodynamic therapy. *Chem Soc Rev*. 2016; 45: 6488-519.
120. Yang X, Yang Y, Gao F, Wei JJ, Qian CG, Sun MJ. Biomimetic Hybrid Nanozymes with Self-Supplied  $\text{H}^+$  and Accelerated  $\text{O}_2$  Generation for Enhanced Starvation and Photodynamic Therapy against Hypoxic Tumors. *Nano Lett*. 2019; 19: 4334-42.
121. Zhou J, Li M, Hou Y, Luo Z, Chen Q, Cao H, et al. Engineering of a Nanosized Biocatalyst for Combined Tumor Starvation and Low-Temperature Photothermal Therapy. *ACS Nano*. 2018; 12: 2858-72.
122. Tang W, Fan W, Zhang W, Yang Z, Li L, Wang Z, et al. Wet/Sono-Chemical Synthesis of Enzymatic Two-Dimensional  $\text{MnO}_2$  Nanosheets for Synergistic Catalysis-Enhanced Phototheranostics. *Adv Mater*. 2019; 31: e1900401.
123. Chen Y, Shi J. Chemistry of Mesoporous Organosilica in Nanotechnology: Molecularly Organic-Inorganic Hybridization into Frameworks. *Adv Mater*. 2016; 28: 3235-72.
124. Chen Y, Xu P, Chen H, Li Y, Bu W, Shu Z, et al. Colloidal HPMO Nanoparticles: Silica-Etching Chemistry Tailoring, Topological Transformation, and Nano-Biomedical Applications. *Adv Mater*. 2013; 25: 3100-5.
125. De Ridder M, Verellen D, Verovski V, Storme G. Hypoxic tumor cell radiosensitization through nitric oxide. *Nitric Oxide-Biol Chem*. 2008; 19: 164-9.
126. Duong HTT, Adnan NNM, Barraud N, Basuki JS, Kutty SK, Jung K, et al. Functional gold nanoparticles for the storage and controlled release of nitric oxide: applications in biofilm dispersal and intracellular delivery. *J Mater Chem B*. 2014; 2: 5003-11.
127. Couzin-Frankel J. Breakthrough of the year 2013. Cancer immunotherapy. *Science*. 2013; 342: 1432-3.
128. Zou W. Immunosuppressive networks in the tumour environment and their therapeutic relevance. *Nat Rev Cancer*. 2005; 5: 263-74.
129. Motz GT, Coukos G. Deciphering and reversing tumor immune suppression. *Immunity*. 2013; 39: 61-73.
130. Xie DL, Wu J, Lou YL, Zhong XP. Tumor suppressor TSC1 is critical for T-cell anergy. *PNAS*. 2012; 109: 14152-7.
131. Chen Q, Wang C, Chen G, Hu Q, Gu Z. Delivery Strategies for Immune Checkpoint Blockade. *Adv Healthc Mater*. 2018; 7: e1800424.
132. Tang L, Zheng Y, Melo MB, Mabardi L, Castano AP, Xie YQ, et al. Enhancing T cell therapy through TCR-signaling-responsive nanoparticle drug delivery. *Nat Biotechnol*. 2018; 36: 707-16.
133. Wang C, Wang J, Zhang X, Yu S, Wen D, Hu Q, et al. *In situ* formed reactive oxygen species-responsive scaffold with gemcitabine and checkpoint inhibitor for combination therapy. *Sci Transl Med*. 2018; 10: eaan3682.
134. Chen Q, Wang C, Zhang X, Chen G, Hu Q, Li H, et al. *In situ* sprayed bioresponsive immunotherapeutic gel for post-surgical cancer treatment. *Nat Nanotechnol*. 2019; 14: 89-97.
135. Yu S, Wang C, Yu J, Wang J, Lu Y, Zhang Y, et al. Injectable Bioresponsive Gel Depot for Enhanced Immune Checkpoint Blockade. *Adv Mater*. 2018; 30: e1801527.
136. Wang C, Sun W, Ye Y, Hu Q, Bomba HN, Gu Z. *In situ* activation of platelets with checkpoint inhibitors for post-surgical cancer immunotherapy. *Nat Biomed Eng*. 2017; 1: 0011-21.

137. Song W, Shen L, Wang Y, Liu Q, Goodwin TJ, Li J, et al. Synergistic and low adverse effect cancer immunotherapy by immunogenic chemotherapy and locally expressed PD-L1 trap. *Nat Commun.* 2018; 9: 2237.
138. Ruan H, Bu L, Hu Q, Cheng H, Lu W, Gu Z. Strategies of Combination Drug Delivery for Immune Checkpoint Blockades. *Adv Healthc Mater.* 2019; 8: 1801099.
139. Zhang YX, Zhao YY, Shen J, Sun X, Liu Y, Liu H, et al. Nanoenabled Modulation of Acidic Tumor Microenvironment Reverses Anergy of Infiltrating T Cells and Potentiates Anti-PD-1 Therapy. *Nano Lett.* 2019; 19: 2774-83.
140. Plebanek MP, Bhaumik D, Bryce PJ, Thaxton CS. Scavenger Receptor Type B1 and Lipoprotein Nanoparticle Inhibit Myeloid-Derived Suppressor Cells. *Mol Cancer Ther.* 2018; 17: 686-97.
141. Yang H, Lu WL, Huang T, Chen QY, Gao J, Zhao Y. An aptamer-Fe<sup>3+</sup> modified nanoparticle for lactate oxidation and tumor photodynamic therapy. *Colloids Surf B Biointerfaces.* 2018; 164: 192-200.
142. Bonuccelli G, Tsirigos A, Whitaker-Menezes D, Pavlides S, Pestell RG, Chiavarina B, et al. Ketones and lactate "fuel" tumor growth and metastasis: Evidence that epithelial cancer cells use oxidative mitochondrial metabolism. *Cell cycle.* 2010; 9: 3506-14.
143. Sonveaux P, Vegran F, Schroeder T, Wergin MC, Verrax J, Rabbani ZN, et al. Targeting lactate-fueled respiration selectively kills hypoxic tumor cells in mice. *J Clin Invest.* 2008; 118: 3930-42.
144. Wang C, Ye Y, Hu Q, Bellotti A, Gu Z. Tailoring Biomaterials for Cancer Immunotherapy: Emerging Trends and Future Outlook. *Adv Mater.* 2017; 29: 1606036.
145. Jin H, Pi J, Yang F, Wu C, Cheng X, Bai H, et al. Ursolic acid-loaded chitosan nanoparticles induce potent anti-angiogenesis in tumor. *Appl Microbiol Biotechnol.* 2016; 100: 6643-52.
146. Pan F, Yang W, Li W, Yang XY, Liu S, Li X, et al. Conjugation of gold nanoparticles and recombinant human endostatin modulates vascular normalization via interruption of anterior gradient 2-mediated angiogenesis. *Tumour Biol.* 2017; 39: 1010428317708547.
147. Choi JY, Ramasamy T, Kim SY, Kim J, Ku SK, Youn YS, et al. PEGylated lipid bilayer-supported mesoporous silica nanoparticle composite for synergistic co-delivery of axitinib and celestrol in multi-targeted cancer therapy. *Acta Biomater.* 2016; 39: 94-105.
148. Yao Z, Zhang B, Liang T, Ding J, Min Q, Zhu JJ. Promoting Oxidative Stress in Cancer Starvation Therapy by Site-Specific Startup of Hyaluronic Acid-Enveloped Dual-Catalytic Nanoreactors. *ACS Appl Mater Interfaces.* 2019; 11: 18995-9005.
149. Du X, Zhang T, Ma G, Gu X, Wang G, Li J. Glucose-responsive mesoporous silica nanoparticles to generation of hydrogen peroxide for synergistic cancer starvation and chemistry therapy. *Int J Nanomedicine.* 2019; 14: 2233-51.
150. Pan W, Ge Y, Yu Z, Zhou P, Cui B, Li N, et al. A cancer cell membrane-encapsulated MnO<sub>2</sub> nanoreactor for combined photodynamic-starvation therapy. *Chem Commun.* 2019; 55: 5115-8.
151. Liu Z, Li T, Han F, Wang Y, Gan Y, Shi J, et al. A cascade-reaction enabled synergistic cancer starvation/ROS-mediated/chemo-therapy with an enzyme modified Fe-based MOF. *Biomater Sci.* 2019; 7: 3683-92.